Cell Metabolism

Article

SGLT2 Inhibition Mediates Protection from Diabetic Kidney Disease by Promoting Ketone Body-Induced mTORC1 Inhibition

Graphical Abstract

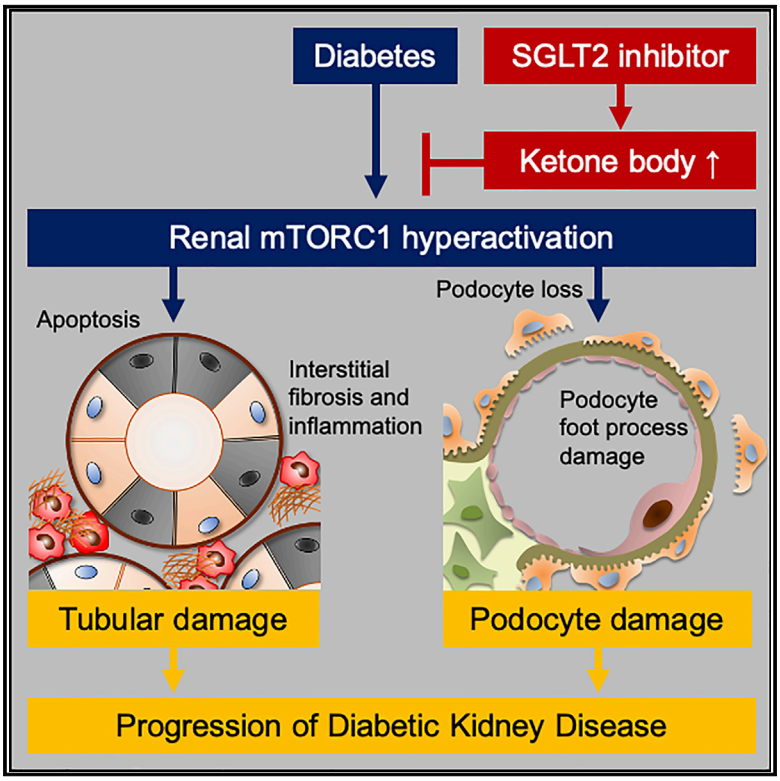

Highlights

- Energy metabolism shifts from lipolysis to ketolysis in damaged kidneys
- mTORC1 hyperactivation leads to impaired renal lipolysis and subsequent renal damage
- Ketone body supplementation ameliorates renal damage by blocking mTORC1 signaling
- SGLT2 inhibitor-mediated renoprotection involves mTORC1 inhibition by ketone bodies

Authors

Issei Tomita, Shinji Kume, Sho Sugahara, ..., Hisakazu Ogita, Shin-ichi Araki, Hiroshi Maegawa

Correspondence

skume@belle.shiga-med.ac.jp (S.K.), maegawa@belle.shiga-med.ac.jp (H.M.)

In Brief

SGLT2 inhibitors have been shown to offer potent renoprotection against diabetic kidney disease. But the mechanism for this effect has been unclear. Here, Tomita et al. report that the drugs promote elevation of ketone bodies, which subsequently inhibit mTORC1 in the proximal renal tubules, explaining their protective effects on this organ.

Tomita et al., 2020, Cell Metabolism *32*, 404–419
September 1, 2020
https://doi.org/10.1016/j.cmet.2020.06.020

CellPress

CellPress

Cell Metabolism

Article

SGLT2 Inhibition Mediates Protection from Diabetic Kidney Disease by Promoting Ketone Body-Induced mTORC1 Inhibition

Issei Tomita,[1] Shinji Kume,[1,8,*] Sho Sugahara,[1] Norihisa Osawa,[1] Kosuke Yamahara,[1] Mako Yasuda-Yamahara,[1] Naoko Takeda,[1,2] Masami Chin-Kanasaki,[1,2] Tatsuroh Kaneko,[3] Eric Mayoux,[4] Michael Mark,[4] Motoko Yanagita,[5,6] Hisakazu Ogita,[7] Shin-ichi Araki,[1,2] and Hiroshi Maegawa[1,*]

[1]Department of Medicine, Shiga University of Medical Science, Tsukinowa-cho, Seta, Otsu, Shiga 520-2192, Japan
[2]Division of Blood Purification, Shiga University of Medical Science Hospital, Tsukinowa-cho, Seta, Otsu, Shiga 520-2192, Japan
[3]Medicine Division, Nippon Boehringer Ingelheim Co., Ltd., 2-1-1 Osaki, Shinagawa-ku, Tokyo 141-6017, Japan
[4]CardioMetabolic Diseases Research, Boehringer Ingelheim Pharma GmbH & Co. KG, Birkendorfer Strasse 65, Biberach an der Riss 88397, Germany
[5]Department of Nephrology, Graduate School of Medicine, Kyoto University, 54 Shogoin-Kawahara-cho, Sakyo-ku, Kyoto 606-8507 Japan
[6]Institute for the Advanced Study of Human Biology (ASHBi), Kyoto University, 54 Shogoin-Kawahara-cho, Sakyo-ku, Kyoto 606-8507 Japan
[7]Division of Molecular Medical Biochemistry, Department of Biochemistry and Molecular Biology, Shiga University of Medical Science, Tsukinowa-cho, Seta, Otsu, Shiga 520-2192, Japan
[8]Lead Contact
*Correspondence: skume@belle.shiga-med.ac.jp (S.K.), maegawa@belle.shiga-med.ac.jp (H.M.)
https://doi.org/10.1016/j.cmet.2020.06.020

SUMMARY

SGLT2 inhibitors offer strong renoprotection in subjects with diabetic kidney disease (DKD). But the mechanism for such protection is not clear. Here, we report that in damaged proximal tubules of high-fat diet-fed ApoE-knockout mice, a model of non-proteinuric DKD, ATP production shifted from lipolysis to ketolysis dependent due to hyperactivation of the mechanistic target of rapamycin complex 1 (mTORC1). We further found that empagliflozin raised endogenous ketone body (KB) levels, and thus its use or treatment with 1,3-butanediol, a KB precursor, prevented decreases in renal ATP levels and organ damage in the mice. The renoprotective effect of empagliflozin was abolished by gene deletion of Hmgcs2, a rate-limiting enzyme of ketogenesis. Furthermore, KBs attenuated mTORC1-associated podocyte damage and proteinuria in diabetic *db/db* mice. Our findings show that SGLT2 inhibition-associated renoprotection is mediated by an elevation of KBs that in turn corrects mTORC1 hyperactivation that occurs in non-proteinuric and proteinuric DKD.

INTRODUCTION

Diabetic kidney disease (DKD) has long been recognized as being associated with progressive proteinuria (de Zeeuw et al., 2004), and preventing massive proteinuria due to glomerular damage remains a challenge in the management of DKD. Even so, the clinical manifestation of DKD has continued to evolve with an increase in the prevalence of nonproteinuric DKD (Afkarian et al., 2016; Kume et al., 2019)—an emerging issue that requires a novel therapeutic strategy. Although the exact mechanism underlying nonproteinuric DKD remains unresolved, atherosclerosis- and hypoxia-related renal tubular damage

Context and Significance

SGLT2 inhibitors, an important class of anti-diabetes drugs, have been found to offer potent protection from kidney disease, a critical comorbidity of diabetes. But how they offer such protection has not been clear. Here, Hiroshi Maegawa, Shinji Kume, and their colleagues show that SGLT2 inhibitors promote the elevation of ketone bodies by enhancing ketogenesis. The ketone bodies, in turn, were shown to act on kidney cells where they inhibit the excess activation of an important energy-sensing intracellular pathway, allowing better function of the organ. Such an effect could be replicated by exogenous supplementation with ketone bodies, even in non-diabetic mouse models of kidney disease. Thus, these findings have broad implications for the potential treatment of kidney pathologies.

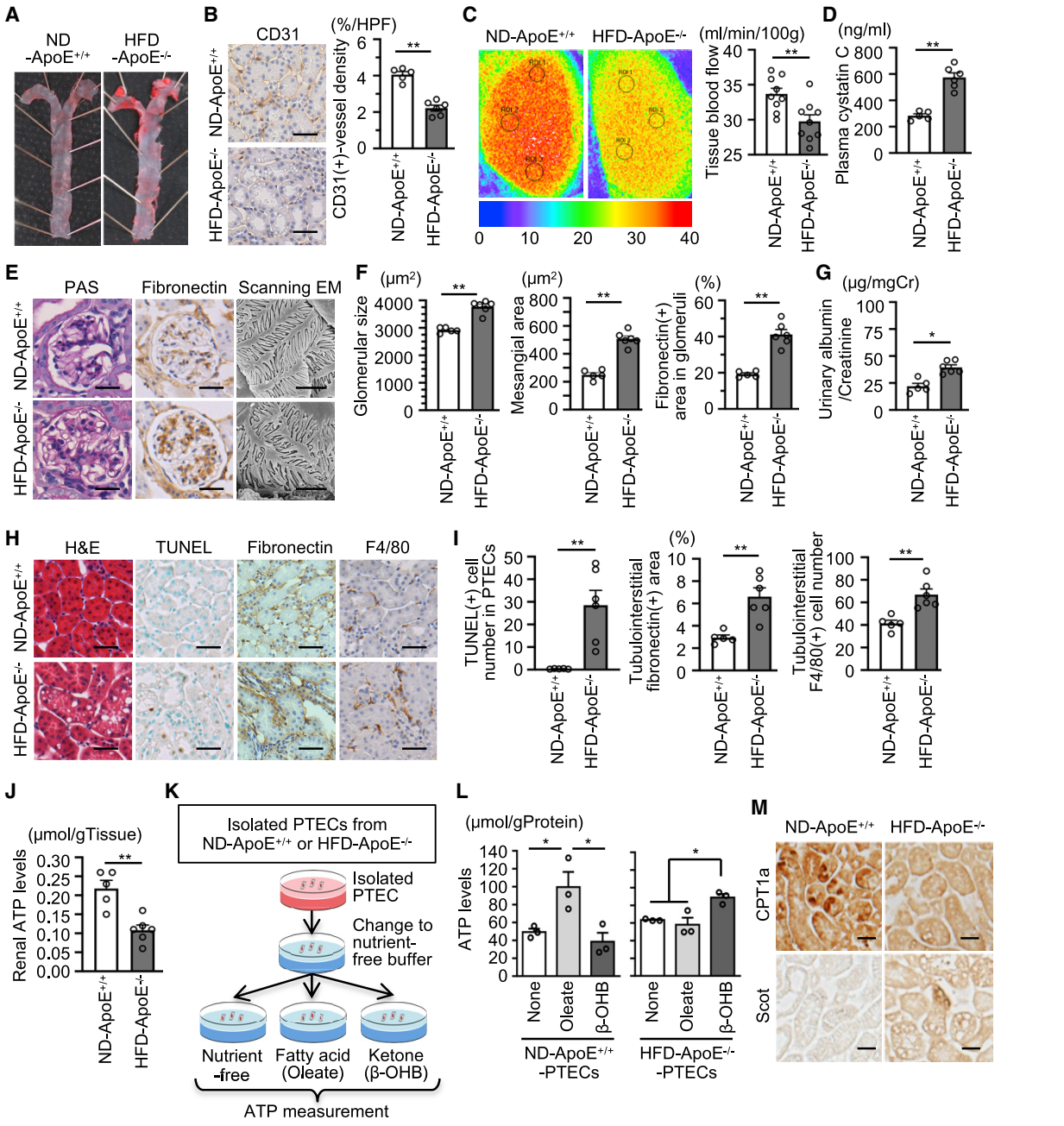

Figure 1. ATP Production Shifts from Lipolysis Dependence to Ketolysis Dependence in PTECs of HFD-Fed *ApoE*$^{-/-}$ Mice

(A) En face analysis of aorta in ND-fed *ApoE*$^{+/+}$ mice and HFD-fed *ApoE*$^{-/-}$ mice.

(B) Representative images of peritubular capillary density determined with CD31 immunostaining (scale bar, 50 μm) and quantitative analysis (20 areas per mouse were analyzed, n = 5–6).

(C) Renal blood flow and quantitative analysis (n = 9 areas per group).

(D) Plasma cystatin C levels.

(E and F) Representative images of PAS and fibronectin staining in glomeruli (scale bar, 25 μm) and scanning electron microscopic analysis of podocytes (scale bar, 2 μm) (E), and quantitative analysis of glomerular size, mesangial area, and fibronectin-positive area (20 glomeruli per mouse were analyzed, n = 5–6) (F).

(G) Urinary albumin excretion levels.

(H) Representative images of H&E staining, TUNEL staining, and immunostaining of fibronectin and F4/80 in renal tubulointerstitial lesions (scale bar, 50 μm) (20 areas per mouse were analyzed, n = 5–6).

(I) Quantitative analysis of TUNEL-positive cell number, fibronectin-positive area, and F4/80-positive cell number in tubulointerstitial lesions.

(J) ATP levels in renal cortex samples.

(legend continued on next page)

(rather than glomerular damage) is suggested to be associated with this type of DKD (Mimura and Nangaku, 2010; Shimizu et al., 2014; Singh et al., 2008). Thus, in addition to developing additional therapies to reduce proteinuria, protecting proximal tubular epithelial cells (PTECs) against atherosclerosis-mediated systemic damage may provide an improved means to improve outcomes in individuals with DKD.

Growing evidence from recent large clinical trials has demonstrated that inhibitors of sodium glucose cotransporter 2 (SGLT2) reduce the risk of heart failure and improve renal endpoints in individuals with diabetes beyond their glucose-lowering effect (Neal et al., 2017; Wanner et al., 2016; Wiviott et al., 2019). Furthermore, sub-analysis of these trials indicated that the inhibitors slowed the decline of renal function for both proteinuric and nonproteinuric DKD (Cherney et al., 2017; Neuen et al., 2019). Thus, revealing the mechanism underlying SGLT2 inhibitor-mediated renoprotection should provide novel insights into the pathogenesis of both these forms of DKD.

Several reno- and cardioprotective mechanisms of SGLT2 inhibitors have been proposed, such as amelioration of tubuloglomerular feedback (Kidokoro et al., 2019), hematocrit elevation (Mazer et al., 2020; Sano et al., 2016), antioxidant properties (Kamezaki et al., 2018; Tanaka et al., 2018), recruitment of progenitor cells (Hess et al., 2019), and vascular remodeling (Zhang et al., 2018). In addition, enhanced ketone body utilization in tissues may be involved in SGLT2 inhibitor-mediated cardio-protection (Ferrannini et al., 2016; Mudaliar et al., 2016). Furthermore, accumulating evidence demonstrates that enhancing ketone body levels can promote beneficial effects on health, such as longer life expectancy (Newman et al., 2017; Roberts et al., 2017), enhanced endurance capacity (Cox et al., 2016), and local tissue repair (Cheng et al., 2019). However, the role of ketone body metabolism in SGLT2 inhibitor-mediated cardioprotection is still under debate (Lopaschuk and Verma, 2016), and its role in renoprotection has not been elucidated.

ATP production is essential for maintaining cell survival and function. PTECs depend largely on lipolysis for ATP production under physiological conditions, whereas the impairment of lipolysis-dependent ATP production is associated with the progression of kidney diseases, including DKD (Kang et al., 2015; Tanaka et al., 2011). Given that ketone bodies are an energy source, ameliorating defective energy metabolism by increasing ketone body levels in damaged PTECs may become a novel therapy for kidney diseases.

Altered intracellular nutrient signals are also involved in the pathogenesis of DKD (Kume et al., 2012). Of these signals, hyperactivation of the mechanistic target of rapamycin complex 1 (mTORC1), which is activated under a hyper-nutrient state, has been reported to be strongly associated with both PTEC and podocyte damage in DKD (Gödel et al., 2011; Inoki et al., 2011; Kuwagata et al., 2016), suggesting that inhibition of overactive mTORC1 signaling may represent a therapy for nonproteinuric and proteinuric DKD. Ketone bodies have recently attracted greater attention because this metabolite can function not only as an ATP source, particularly during fasting, but also as a direct modulator of intracellular nutrient signals (Puchalska and Crawford, 2017). Thus, we hypothesized that, in addition to being a direct energy source for damaged PTECs, ketone bodies prevent PTEC and podocyte damage by inhibiting mTORC1 signaling as a signal mediator of fasting, and that this mechanism may explain how SGLT2 inhibitors mediate renoprotection.

The present study was designed to verify this hypothesis using both high-fat diet (HFD)-fed *ApoE* knockout ($ApoE^{-/-}$) mice as a model of nonproteinuric DKD with atherosclerosis and *db/db* mice as a model of proteinuric DKD. We report here that ketone bodies exert renoprotective properties by inhibiting mTORC1 signaling in PTECs and podocytes, and that this at least partially explains the mechanism of SGLT2 inhibitor-mediated renoprotection in nonproteinuric and proteinuric DKD.

RESULTS

ATP Production Shifts from a Lipolysis to a Ketolysis Dependence in PTECs of HFD-Fed $ApoE^{-/-}$ Mice

HFD-fed $ApoE^{-/-}$ mice (aged 34 weeks) showed obesity-related hyperglycemia when compared with that of normal diet (ND)-fed $ApoE^{+/+}$ mice (183 ± 15 mg/dL versus 118 ± 12 mg/dL, $p < 0.05$). HFD-fed $ApoE^{-/-}$ mice developed aortic atherosclerosis, and lower CD31-positive peritubular capillary density and renal blood flow (Figures 1A–1C). To evaluate renal function, we measured plasma cystatin C levels in mice (Leelahavanichkul et al., 2014). HFD-fed $ApoE^{-/-}$ mice exhibited renal dysfunction defined by high levels of plasma cystatin C (Figure 1D). In this model, we found glomerular hypertrophy and mesangial expansion with fibrosis (Figures 1E and 1F); however, podocyte damage, as determined by scanning electron microscopy, was not detected (Figure 1E), and albuminuria was very mild (Figure 1G). In contrast to mild albuminuria, PTEC damage with vacuolar changes, as based on hematoxylin and eosin (H&E) staining, and apoptosis, as well as tubulointerstitial fibrosis and inflammation, were severe in the mice (Figures 1H and 1I). Thus, HFD-fed $ApoE^{-/-}$ mice exhibited a renal phenotype of nonproteinuric renal dysfunction with relatively advanced tubulointerstitial lesions accompanied by macro- and microvascular damage rather than a renal phenotype indicative of massive proteinuria. We believe this mouse model successfully reflects human nonproteinuric DKD, which can be associated with atherosclerosis.

Renal ATP levels in the kidneys of HFD-fed $ApoE^{-/-}$ mice were lower than those of ND-fed $ApoE^{+/+}$ mice (Figure 1J). When we analyzed dependence on fatty acids (oleate) and ketone bodies (β-hydroxybutyrate; β-OHB) for ATP production using isolated PTECs from either ND-fed $ApoE^{+/+}$ or HFD-fed $ApoE^{-/-}$ mice (Figure 1K), ATP production in PTECs from healthy and damaged kidneys was dependent on lipolysis and ketolysis, respectively (Figure 1L). When compared to ND-fed $ApoE^{+/+}$ mice, HFD-fed $ApoE^{-/-}$ mice exhibited lower renal expression of carnitine palmitoyltransferase 1a (CPT1a), a lipolytic enzyme, and higher renal expression of succinyl-CoA-3-oxaloacid CoA transferase

(K) Protocol to examine energy dependency on oleate or β-OHB in isolated PTECs.
(L) ATP levels after treatment with either oleate or β-OHB in isolated PTECs.
(M) Immunostaining of CPT1a and Scot in kidney samples (scale bar, 50 μm).
Data are represented as mean ± SEM. *$p < 0.05$, **$p < 0.01$.

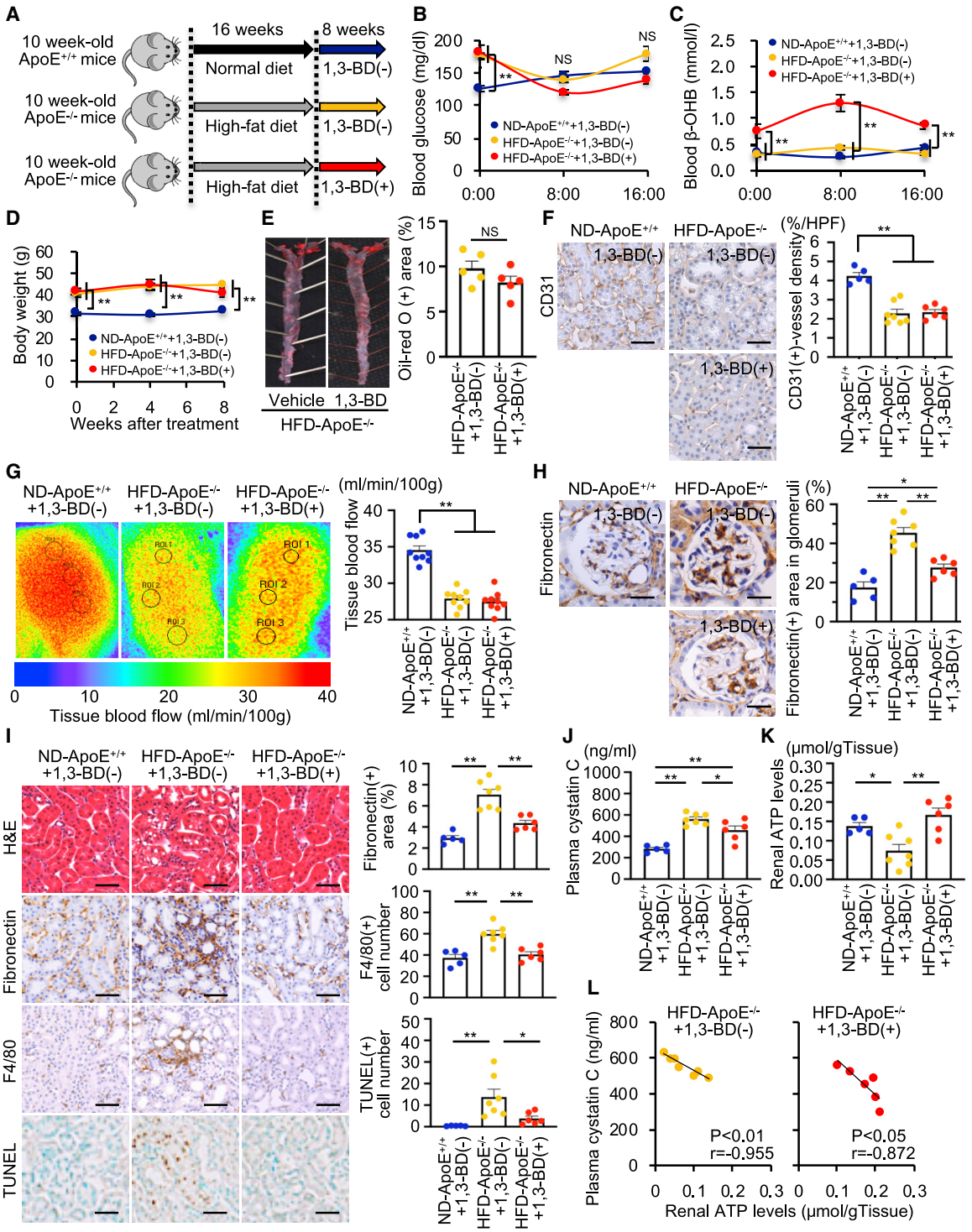

Figure 2. Ketone Body Supplementation with 1,3-Butanediol (1,3-BD) Ameliorates Kidney Injury in HFD-Fed *ApoE*$^{-/-}$ Mice

(A) Study protocol for examining the effect of 1,3-BD on the renal phenotype of HFD-fed *ApoE*$^{-/-}$ mice.

(B and C) Daily profiles of blood glucose (B) and β-OHB (C) (n = 5–7).

(D) Body weight change during the experimental period.

(E) Representative images of en face analysis to detect atherosclerosis, and quantitative data (n = 5 total samples analyzed, per group).

(F) Representative images of peritubular capillary density determined with CD31 immunostaining (scale bar, 50 μm) and quantitative analysis (20 areas per mouse were analyzed, n = 5–7).

(G) Renal blood flow and quantitative analysis (n = 9 areas per group).

(legend continued on next page)

(Scot), a ketolysis-related enzyme. (Figure 1M), suggesting that the energy generation of damaged PTECs shifted from lipolysis to ketolysis dependence.

Supplementation with 1,3-Butanediol (1,3-BD) Ameliorates Kidney Injury in HFD-Fed *ApoE*$^{-/-}$ Mice

1,3-BD is a chemical ketone body precursor that can be orally administered and is converted to β-OHB in the liver in an insulin-independent manner. We first confirmed that 1,3-BD increased blood β-OHB levels without affecting blood glucose levels in control C57BL/6 mice (Figures S1A–S1C) and did not show any evidence of renotoxicity (Figures S1D and S1E). Subsequently, 1,3-BD was administered to HFD-fed *ApoE*$^{-/-}$ mice (Figure 2A). 1,3-BD treatment significantly increased blood β-OHB levels without affecting blood glucose levels in HFD-fed *ApoE*$^{-/-}$ mice (Figures 2B and 2C). This treatment did not alter body weight gain, blood pressure, blood pH, or lipid profiles of HFD-fed *ApoE*$^{-/-}$ mice (Figure 2D; Table S1). Furthermore, 1,3-BD treatment did not improve macro- and intrarenal microvascular damage, and accordingly did not alter reduced renal blood flow in HFD-fed *ApoE*$^{-/-}$ mice (Figures 2E–2G).

In contrast to the effect on vascular damage, 1,3-BD treatment significantly prevented glomerular damage, tubular vacuolar formation, tubulointerstitial fibrosis and inflammation, PTEC apoptosis, mitochondrial morphological changes (round shape and fragmentation) in PTECs, and subsequent renal dysfunction as assessed by measuring plasma cystatin C levels (Figures 2H–2J and S1F). Furthermore, 1,3-BD treatment restored renal ATP levels in HFD-fed *ApoE*$^{-/-}$ mice (Figure 2K), and renal ATP levels were inversely correlated with plasma cystatin C levels in HFD-fed *ApoE*$^{-/-}$ mice treated with or without 1,3-BD (Figure 2L). These findings suggest that increasing ketone bodies ameliorates vascular damage-related kidney injury in diabetic mice, which is accompanied by restoration of renal ATP production.

Empagliflozin Restores Renal ATP Levels and Ameliorates Kidney Injury in HFD-Fed *ApoE*$^{-/-}$ Mice

When we examined the effects of empagliflozin, an SGLT2 inhibitor used clinically, on kidney injury in HFD-fed *ApoE*$^{-/-}$ mice under *ad libitum* feeding (Figure S2A), we found that blood glucose levels were lower than the non-treated group (Figure S2B), but blood ketone body levels were not different, and vascular damage-related renal tissue damage and dysfunction were not ameliorated (Figures S2C–S2E).

Endogenous ketone body production from the liver is physiologically suppressed by postprandial insulin action, and increased blood ketone levels by an SGLT2 inhibitor were predominantly observed after overnight fasting in human subjects (Ferrannini et al., 2016). Thus, we considered that complete fasting during sleep is required to increase plasma ketone body levels by SGLT2 inhibitors in an animal study. We then performed a preliminary examination of the effect of empagliflozin treatment, along with complete dietary withdrawal for 8 h during a sleeping period, on blood glucose and β-OHB levels in C57BL/6 mice (Figure S2F). We confirmed that this protocol of empagliflozin administration successfully increased blood β-OHB levels during fasting, without altering fasting blood glucose levels and any renal adverse effects (Figures S2G–S2J).

Thus, we verified the effectiveness of empagliflozin in kidney injury in HFD-fed *ApoE*$^{-/-}$ mice using this protocol (Figure 3A). This treatment significantly decreased blood glucose levels and increased ketone body levels after fasting in 26- and 30-week-old HFD-fed *ApoE*$^{-/-}$ mice (Figures 3B, 3C, S2K, and S2L). Long-term treatment with empagliflozin lowered body weight but did not affect blood pressure, plasma pH, or lipid profiles in HFD-fed *ApoE*$^{-/-}$ mice (Figure 3D; Table S2). This strategy suppressed the development of aortic atherosclerosis (Figure 3E), whereas CD31-positive peritubular capillary density loss and renal blood flow were not restored (Figures 3F and 3G). When we analyzed aortic atherosclerosis and peritubular capillary density in 26-week-old HFD-fed *ApoE*$^{-/-}$ mice (before starting the empagliflozin treatment), aortic atherosclerosis was still mild, but peritubular capillary density loss was already established when compared with those in 34-week-old HFD-fed *ApoE*$^{-/-}$ mice (Figure S2M). Thus, it was possible that empagliflozin treatment prevented further development of aortic atherosclerosis from 26 to 34 weeks of age, and was not able to reverse the established renal peritubular capillary loss.

Even in kidneys where renal blood flow was not restored in 34-week-old HFD-fed *ApoE*$^{-/-}$ mice, empagliflozin prevented glomerular damage, tubular cell alteration and apoptosis, tubulointerstitial fibrosis and inflammation, mitochondrial abnormalities in PTECs, and elevation of plasma cystatin C levels (Figures 3H–3J and S2N). Furthermore, empagliflozin treatment restored renal ATP levels (Figure 3K), which were associated with improved renal function (Figure 3L). Thus, SGLT2 inhibitor treatment showed a similar renoprotective effect as 1,3-BD administration.

Hmgcs2 Deficiency Abolishes Empagliflozin-Mediated Renoprotection in HFD-Fed *ApoE*$^{-/-}$ Mice

To confirm the importance of endogenous ketogenesis in the renoprotection elicited by SGLT2 inhibition, we generated mice lacking the *Hmgcs2* gene, which encodes the rate-limiting enzyme of endogenous ketogenesis, using the Crispr-CAS9 system to delete a part of exon 2 (Figure 4A). The resulting frameshift of *Hmgcs2* caused complete deletion of hepatic Hmgcs2 protein expression (Figure 4B), and impaired both fasting-dependent and SGLT2 inhibitor-dependent ketogenesis without affecting glucose metabolism (Figures 4C–4F). We found that *Hmgcs2* deficiency alone neither exacerbated kidney injury nor decreased renal ATP levels in HFD-fed *ApoE*$^{-/-}$ mice, although

(H) Representative images of immunostaining of fibronectin in glomeruli (scale bar, 25 μm) and quantitative analysis (20 glomeruli per mouse were analyzed, n = 5–7).
(I) Representative images of H&E staining, immunostaining of fibronectin and F4/80, and TUNEL staining in tubulointerstitial lesions (scale bar, 50 μm), and quantitative analysis (20 areas per mouse were analyzed, n = 5–7).
(J and K) Plasma cystatin C (J) and renal ATP levels in renal cortex samples (K).
(L) Correlation analysis between plasma cystatin C and renal ATP levels.
Data are represented as mean ± SEM. *p < 0.05, **p < 0.01. NS indicates no significance.

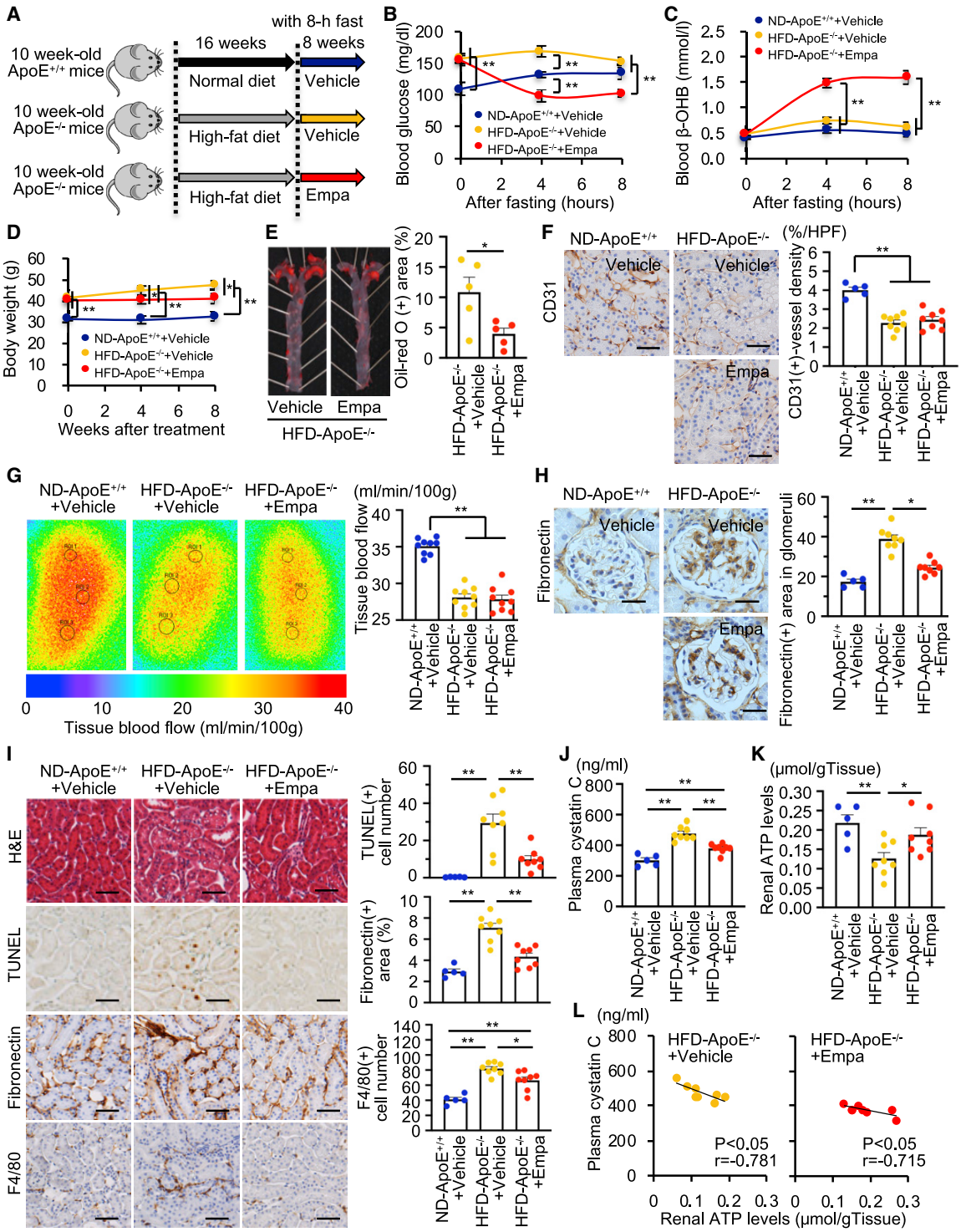

Figure 3. Empagliflozin Restores Renal ATP levels and Ameliorates Kidney Injury in HFD-Fed *ApoE*$^{-/-}$ Mice

(A) Study protocol for examining the effect of empagliflozin (Empa) on the renal phenotype of HFD-fed *ApoE*$^{-/-}$ mice.

(B and C) Changes in blood glucose (B) and β-OHB (C) during 8-h fasting (n = 5–8).

(D) Body weight change during the experimental period.

(E) Representative images of en face analysis of the aorta and quantitative analysis (n = 5 total samples analyzed per group).

(F) Representative images of peritubular capillary density determined with CD31 immunostaining (scale bar, 50 μm) and quantitative analysis (20 areas per mouse were analyzed, n = 5–8).

(G) Renal blood flow and quantitative analysis (n = 9 areas per group).

(legend continued on next page)

the gene deletion decreased blood β-OHB levels without affecting blood glucose levels (Figures S3A–S3F), suggesting that further lowering the originally low ketone body concentration by *Hmgcs2* deficiency did not aggravate renal damage.

We next generated double-knockout mice lacking both *ApoE* and *Hmgcs2* genes. The double-knockout mice were treated with empagliflozin under HFD-fed conditions with 8-h fasting daily, to examine the effect of *Hmgcs2* gene deletion on empagliflozin-mediated renoprotection in HFD-fed *ApoE*$^{-/-}$ mice (Figure 4G). Metabolic characteristics of the study groups are shown in Table S3. Although *Hmgcs2* deficiency did not alter changes in body weight or the anti-atherogenic effect of empagliflozin in HFD-fed *ApoE*$^{-/-}$ mice (Figures 4H and 4I), deletion of this gene abolished empagliflozin-mediated renoprotection and restoration of renal ATP production without affecting the decrease in CD31-positive peritubular capillary density (Figures 4J–4M and S3G). Thus, enhanced endogenous ketogenesis is required for the renoprotective action of SGLT2 inhibitors against vascular damage-related kidney injury.

Hyperactivation of mTORC1 Impairs Renal Lipolysis in PTECs of HFD-Fed *ApoE*$^{-/-}$ Mice

We next examined the effect of ketone body supplementation on the relationship between mTORC1 signaling and renal lipolysis in DKD, as hyperactivation of mTORC1 signaling is reportedly involved in both the pathogenesis of DKD (Gödel et al., 2011; Inoki et al., 2011; Kuwagata et al., 2016) and impairment of lipolysis in some tissues (Ricoult and Manning, 2013). In the kidneys of control ND-fed *ApoE*$^{+/+}$ mice, mTORC1 signaling (as assessed by phosphorylation of the S6 protein) was inactive in aquaporin 1 (AQP1)-positive PTECs, but was active in calbindin D28k (CaBP)-positive distal tubules even under healthy conditions (Figure 5A). In HFD-fed *ApoE*$^{-/-}$ mice, mTORC1 activity in the PTECs and distal tubules was activated and enhanced, respectively (Figure 5A). 1,3-BD treatment attenuated mTORC1 signaling in both PTECs and distal tubules of HFD-fed *ApoE*$^{-/-}$ mice, although it did not suppress the basal level of mTORC1 activity in distal tubules (Figure 5A). Furthermore, empagliflozin treatment with 8-h fasting suppressed renal mTORC1 hyperactivation, but this effect was abolished by deletion of the *Hmgcs2* gene (Figure 5A). These findings were confirmed by immunoblot analysis (Figure 5B).

Rapamycin, an inhibitor of mTORC1, significantly prevented mTORC1 hyperactivation and recovered fatty acid (oleate)-derived ATP production, but did not suppress ketolysis-dependent ATP production in PTECs isolated from HFD-fed *ApoE*$^{-/-}$ mice (Figures 5C and 5D). In the kidneys of HFD-fed *ApoE*$^{-/-}$ mice, both 1,3-BD treatment and empagliflozin restored CPT1a expression but did not affect Scot expression (Figures 5E and 5F). These results suggest that mTORC1 hyperactivation is associated with decreased renal lipolysis but is not involved in enhanced renal ketolysis associated with DKD.

1,3-BD and Empagliflozin Ameliorate Kidney Injury and the Mortality Rate in Tamoxifen-Inducible Kidney Tubule-Specific *Tsc-1* Knockout (Kidney-*Tsc1*$^{-/-}$) Mice

To further confirm the effect of ketone bodies on mTORC1 inhibition, we generated kidney-*Tsc1*$^{-/-}$ mice using *Tsc1*$^{f/f}$ mice and tamoxifen-inducible kidney-specific (Ndrg1 promoter-derived) Cre^{ERT2}-expressing mice (Endo et al., 2015). In this mouse model, hyperactivation of mTORC1 signaling can be induced in renal tubules after tamoxifen injection as Tsc1 inhibits mTORC1 signaling (Inoki et al., 2012; Saxton and Sabatini, 2017).

We analyzed the effect of 1,3-BD on renal mTORC1 activity and renal phenotypes of this mouse model (Figure 6A). *Tsc1* deficiency promoted renal hypertrophy, tubular dilatation, and fibrosis, and it increased serum cystatin C, which was accompanied by enhanced phosphorylation of S6 protein mainly in PTECs (Figures 6B–6E). 1,3-BD treatment significantly attenuated renal hyperactivation of mTORC1, and subsequent renal enlargement and injury (Figures 6B–6E). Furthermore, renal ATP levels in kidney-*Tsc1*$^{-/-}$ mice were lower than those in *Tsc1*$^{f/f}$ mice, but 1,3-BD-mediated ketone body supply prevented ATP production in kidney-*Tsc1*$^{-/-}$ mice (Figure 6F). Kidney-*Tsc1*$^{-/-}$ mice started to die within 5 weeks after tamoxifen-induced *Tsc1* deletion, but the high mortality rate was not found in kidney-*Tsc1*$^{-/-}$ mice treated with 1,3-BD (Figure 6G).

Pretreatment with rapamycin and β-OHB suppressed hyperactivation of mTORC1 in *Tsc1*-deficient cultured PTECs (Figure 6H). *Tsc1* deletion-mediated mTORC1 activation promoted renal metabolic reprograming, as indicated by a reduction in lipolysis and an increase in ketolysis (Figure 6I). Pretreatment with either rapamycin or β-OHB recovered lipolysis, but did not affect enhanced ketolysis, in *Tsc1*-deficient PTECs (Figure 6I). Furthermore, CPT1a expression was lower and Scot expression was higher in kidneys of kidney-*Tsc1*$^{-/-}$ mice, compared with control *Tsc1*$^{f/f}$ mice (Figure S4A). 1,3-BD treatment prevented a decrease in CPT1a expression without affecting Scot expression in kidneys of kidney-*Tsc1*$^{-/-}$ mice (Figure S4A).

We also examined the effect of empagliflozin with 8-h fasting on renal phenotype and mortality rate of kidney-*Tsc1*$^{-/-}$ mice (Figure 6J). Similar to the results observed with 1,3-BD treatment, empagliflozin suppressed mTORC1 activity in PTECs (Figure 6K), ameliorated renal hypertrophy and renal dysfunction (Figures 6L and 7M), and restored renal ATP levels with high levels of CPT1a expression (Figures 6N and S4B) in kidney-*Tsc1*$^{-/-}$ mice. Empagliflozin also prevented a high mortality rate in kidney-*Tsc1*$^{-/-}$ mice (Figure 6O).

1,3-BD Treatment and Empagliflozin Prevent Podocyte Injury and Massive Proteinuria in Type 2 Diabetic *db/db* Mice

As mTORC1 is involved in the development of podocyte injury-related massive proteinuria in DKD, we hypothesized that ketone

(H) Representative images of immunostaining of fibronectin in glomeruli (scale bar, 25 μm) and quantitative analysis (20 glomeruli per mouse were analyzed, n = 5–8).

(I) Representative images of H&E staining, TUNEL staining, and immunostaining of fibronectin and F4/80 in tubulointerstitial lesions (scale bar, 50 μm), and quantitative data (20 areas per mouse were analyzed, n = 5–8).

(J and K) Plasma cystatin C (J) and renal ATP levels in renal cortex samples (K)

(L) Correlation analysis between plasma cystatin C and renal ATP levels.

Data are represented as mean ± SEM. *p < 0.05, **p < 0.01. NS indicates no significance.

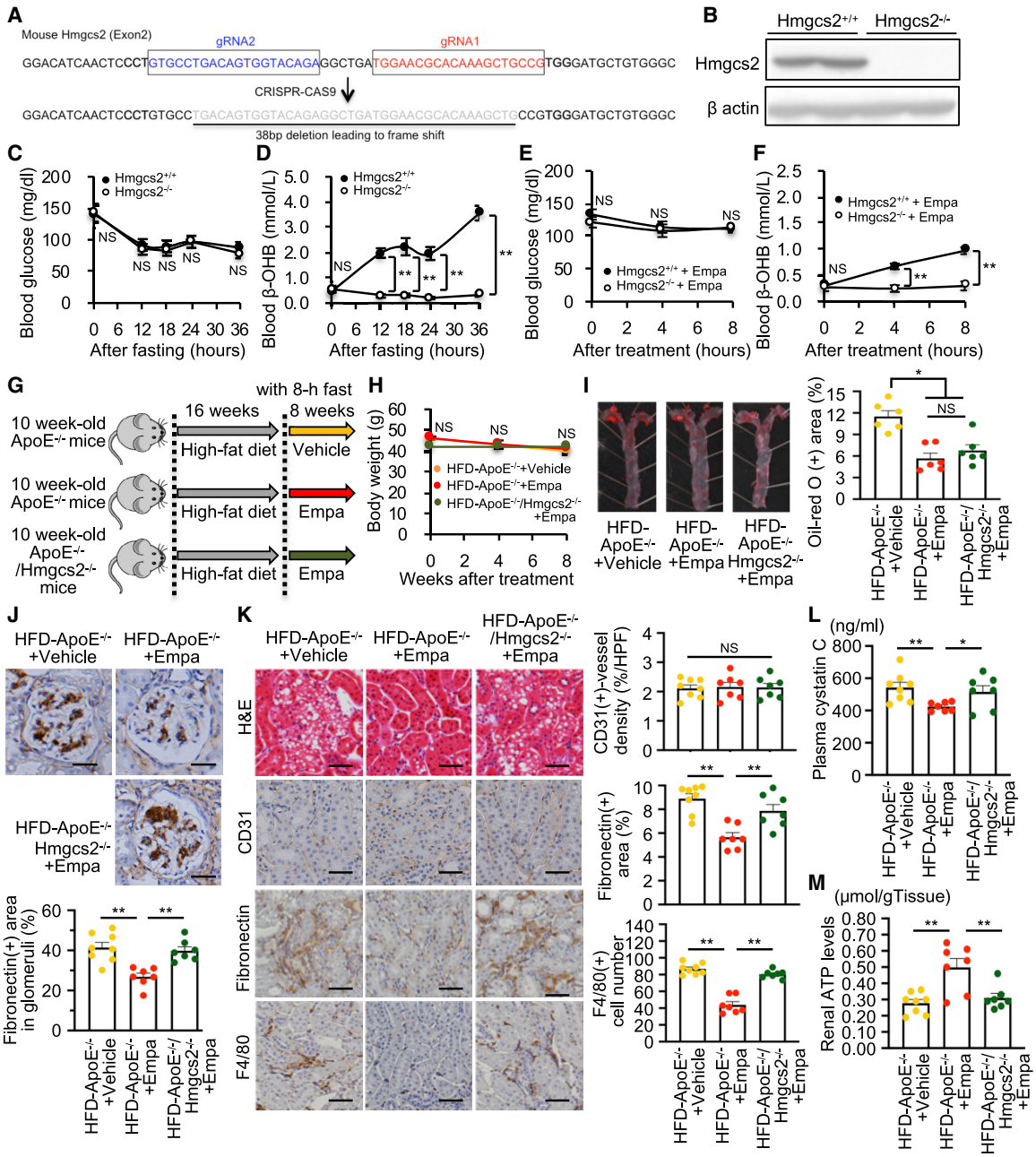

Figure 4. *Hmgcs2* Deficiency Abolishes Empagliflozin-Mediated Renoprotection in HFD-Fed *ApoE*$^{-/-}$ Mice

(A) Generation of an *Hmgcs2* gene-deleted mouse model using the CRISPR-CAS9 system. Two guide RNAs were designed for exon 2 of the gene.

(B) Protein expression of Hmgcs2 in livers of *Hmgcs2*$^{+/+}$ and *Hmgcs2*$^{-/-}$ mice.

(C and D) Fasting-dependent changes in blood glucose (C) and β-OHB (D) in *Hmgcs2*$^{+/+}$ and *Hmgcs2*$^{-/-}$ mice (n = 4–8).

(E and F) Time-dependent changes in blood glucose (E) and β-OHB (F) after empagliflozin treatment in *Hmgcs2*$^{+/+}$ and *Hmgcs2*$^{-/-}$ mice (n = 4–8).

(G) Study protocol for examining the effects of the *Hmgcs2* gene deletion on Empa-mediated renoprotection.

(H) Body weight change during the experimental period (n = 7–8).

(I) Representative images of en face analysis of the aorta and quantitative analysis (n = 6 total samples, per group).

(J) Representative images of immunostaining of fibronectin in glomeruli (scale bar, 25 μm) and quantitative analysis (20 glomeruli per mouse were analyzed, n = 7–8).

(K) Representative images of H&E staining; immunostaining of CD31, fibronectin, and F4/80 in tubulointerstitial lesions (scale bar, 50 μm); and quantitative analysis (20 areas per mouse were analyzed, n = 7–8).

(L and M) Plasma cystatin C (L) and renal ATP levels in renal cortex samples (M).

Data are represented as mean ± SEM. *p < 0.05, **p < 0.01. NS indicates no significance.

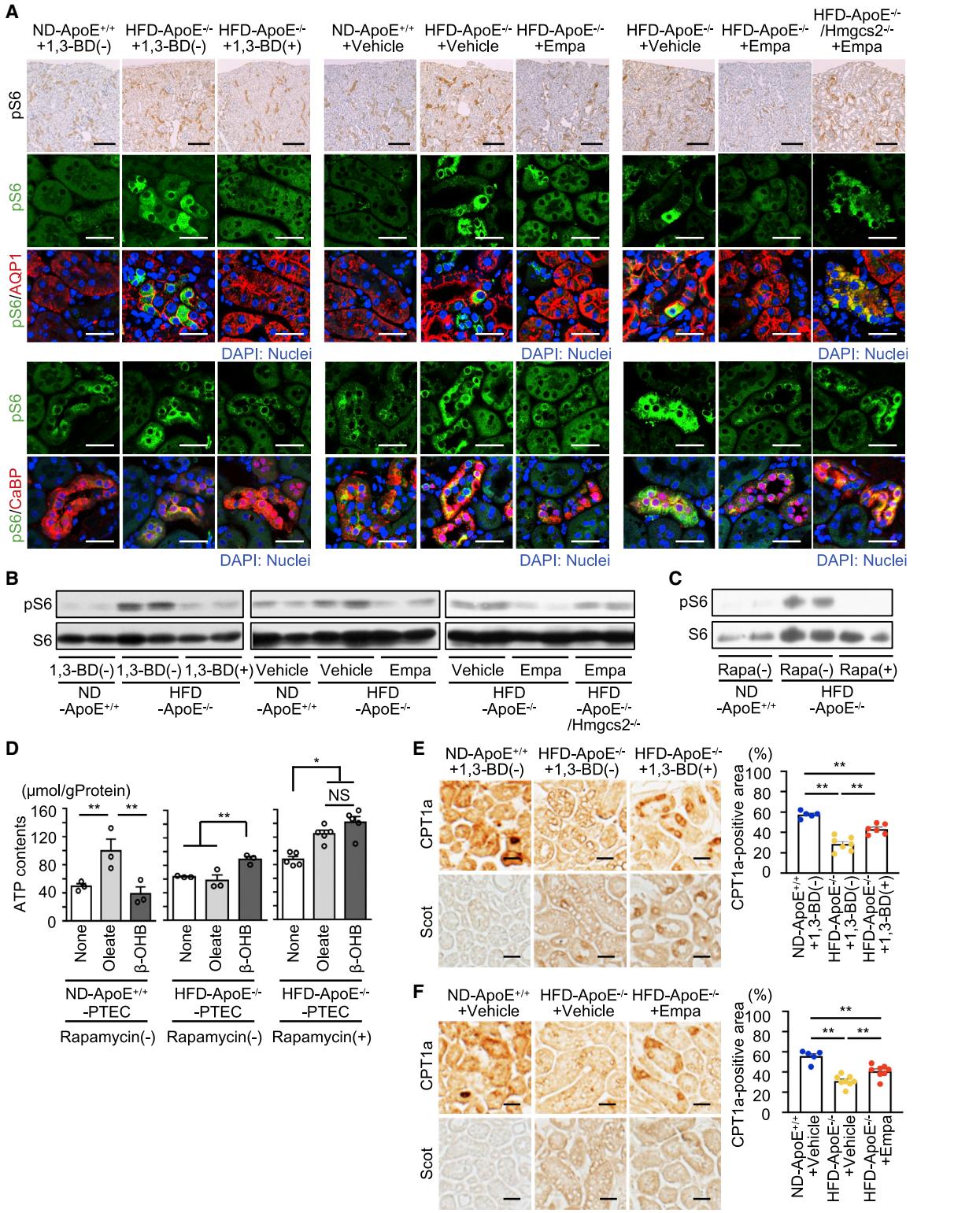

Figure 5. Hyperactivation of mTORC1 Impairs Renal Lipolysis in PTECs of HFD-Fed *ApoE*$^{-/-}$ Mice

(A) Immunohistochemistry of pS6 (scale bar, 500 μm) and immunofluorescent staining of pS6 in AQP1-positive PTECs and Calbindin D28k (CaBP)-positive distal tubules (scale bar, 50 μm).

(B) Representative images of immunoblots for pS6 and S6 in renal cortex samples (n = 5–8 total samples per group analyzed).

(C) Representative images of immunoblots for pS6 and S6 in isolated PTECs (n = 8 total samples per group analyzed).

(legend continued on next page)

body supplementation can prevent podocyte injury in a proteinuric DKD model. In *db/db* mice (a proteinuric DKD model) treated with 1,3-BD (Figure 7A), blood glucose levels were not altered, whereas β-OHB levels were higher than the non-treated *db/db* mice. (Figures S5A and S5B). The treatment reduced massive albuminuria in *db/db* mice (Figure 7B). This treatment also ameliorated fibrosis in both glomerular and interstitial lesions, alteration of podocyte foot process in scanning electron microscopy, and low number of WT1-positive podocyte (Figures 7C–7F), which was accompanied by suppression of mTORC1 signaling in podocytes and renal tubules of *db/db* mice (Figures 7G and S5C). Similarly, empagliflozin with 8-h fasting prevented mTORC1-associated kidney injury in *db/db* mice, with a reduction in blood glucose levels and an increase in β-OHB levels (Figures 7H–7N and S5D–S5F).

1,3-BD Treatment and Empagliflozin Attenuate Kidney Injury in Non-Diabetic 5/6 Nephrotomized Mice

Because the renoprotective potency of SGLT2 inhibitors is expected to occur in non-diabetic kidney diseases, we finally evaluated the effect of 1,3-BD administration and empagliflozin treatment with 8-h fasting on kidney injury in 5/6 nephrectomized mice (Figure S6A). Blood β-OHB levels were higher in the 5/6 nephrectomized mice treated with either 1,3-BD or empagliflozin, compared with non-treated mice (Figure S6B). The treated mice exhibited lower blood pressure, albuminuria, and plasma cystatin C levels (Figures S6C–S6E), with the amelioration of histological damage in both podocytes and tubulointerstitial lesions (Figures S6F and S6G). These ameliorations were accompanied by inhibition of mTORC1 signaling in podocytes and PTECs and maintenance of renal CPT1a expression (Figures S6F and S6G). Scot expression was lower in the damaged kidneys of 5/6 nephrectomized mice, which was not attenuated by the treatments (Figure S6G). These results were consistent with the results obtained from the series of DKD studies outlined above.

DISCUSSION

Growing evidence suggests that elevated ketone bodies have various beneficial effects on health such as increased endurance capacity in athletes and improved cardiac function in heart failure (Cox et al., 2016; Nielsen et al., 2019). The present study demonstrated that ketone bodies exert renoprotective action in DKD and non-DKD models, providing additional support to this concept. Ketone body utilization increases in skeletal muscles during exercise and experimentally in damaged heart tissues (Cox et al., 2016; Nielsen et al., 2019; Schugar et al., 2014; Winder et al., 1974). Similarly, the present study revealed that metabolic reprograming, characterized by a shift from lipolysis to ketolysis, occurred in damaged PTECs. Ketone bodies have long been considered an undesirable metabolite in diabetes because of the life-threatening diabetic ketoacidosis in patients with type 1 diabetes. However, supplying ketone bodies within an optimal range to organs requiring ketone bodies for maintenance of their energy homeostasis is likely to be beneficial for health.

Although the role of ketone body metabolism in SGLT2 inhibitor-mediated organ protection has received significant attention, its exact role has long been debated (Lopaschuk and Verma, 2016). In our study, SGLT2 inhibitor treatment under *ad libitum* feeding did not increase blood ketone body levels and failed to show renoprotection. In contrast, treatment with 8-h daily fasting improved kidney injury, which was accompanied by an increase in ketone body levels. Furthermore, the renoprotective action of an SGLT2 inhibitor was abolished by impaired ketogenesis in *Hmgcs2*-deficient mice. Thus, elevated ketone body levels, as well as the previously proven mechanisms (Kamezaki et al., 2018; Kidokoro et al., 2019; Sano et al., 2016; Tanaka et al., 2018; Zhang et al., 2018), are likely to be involved in the SGLT2 inhibitor-mediated renoprotective effect beyond their glucose-lowering effect in, at least, animal models.

HFD-fed *ApoE*$^{-/-}$ mice developed tubular cell damage and renal dysfunction without massive albuminuria and podocyte injury, representing a model of nonproteinuric DKD with atherosclerosis and intrarenal peritubular capillary density loss, suggesting that this model may be an ideal experimental model for studying vascular damage-related kidney injury with obesity and hyperglycemia. In this mouse model, empagliflozin ameliorated atherosclerosis, but 1,3-BD did not improve atherosclerosis. Systemic improvements, such as body weight reduction and blood glucose lowering, may be associated with the anti-atherosclerotic effect of empagliflozin, and ketone bodies per se are unlikely to have a protective effect against atherosclerosis.

In previous animal studies, the anti-atherosclerotic effect of anti-diabetic drugs has been observed in relatively short-term experiments (Ma et al., 2018; Wang et al., 2017), but human studies have reported that it takes a long time to see the effect of lowering blood glucose levels on atherosclerosis (Holman et al., 2008). As for SGLT2 inhibitors, during the observation period in human clinical studies, the anti-atherosclerosis effect of SGLT2 inhibitors was not evident (Neal et al., 2017; Zinman et al., 2015). However, given that SGLT2 inhibitors ameliorated atherosclerosis in our present data and previous animal studies (Dimitriadis et al., 2019; Han et al., 2017), the anti-atherosclerotic effect via the hypoglycemic effect of the agents may be expected in future follow-up periods in human studies. The explanation for the difference in anti-atherosclerotic effects of anti-diabetic drugs between mice and humans remains unknown.

Ketone bodies have recently been seen as a possible metabolic intermediary in caloric restriction. Ketone bodies have long been recognized as a simple carrier of energy to peripheral tissues from the liver. However, accumulating evidence suggests that ketone bodies act as signaling modulators (Cheng et al., 2019; Puchalska and Crawford, 2017). Several intracellular signals are altered by a ketogenic diet or caloric restriction (Puchalska and Crawford, 2017). Of these, mTORC1 is one of the signals that can be modulated by these nutrient conditions (Inoki

(D) Energy dependency on oleate and β-OHB for the indicated conditions of isolated cells.
(E and F) Representative images of immunostaining of CPT1a and Scot, and quantitative data of a CPT1a-positive area in tubules (scale bar, 50 μm) (20 areas per mouse were analyzed, n = 5–8).
Data are represented as mean ± SEM. *$p < 0.05$, **$p < 0.01$. NS indicates no significance.

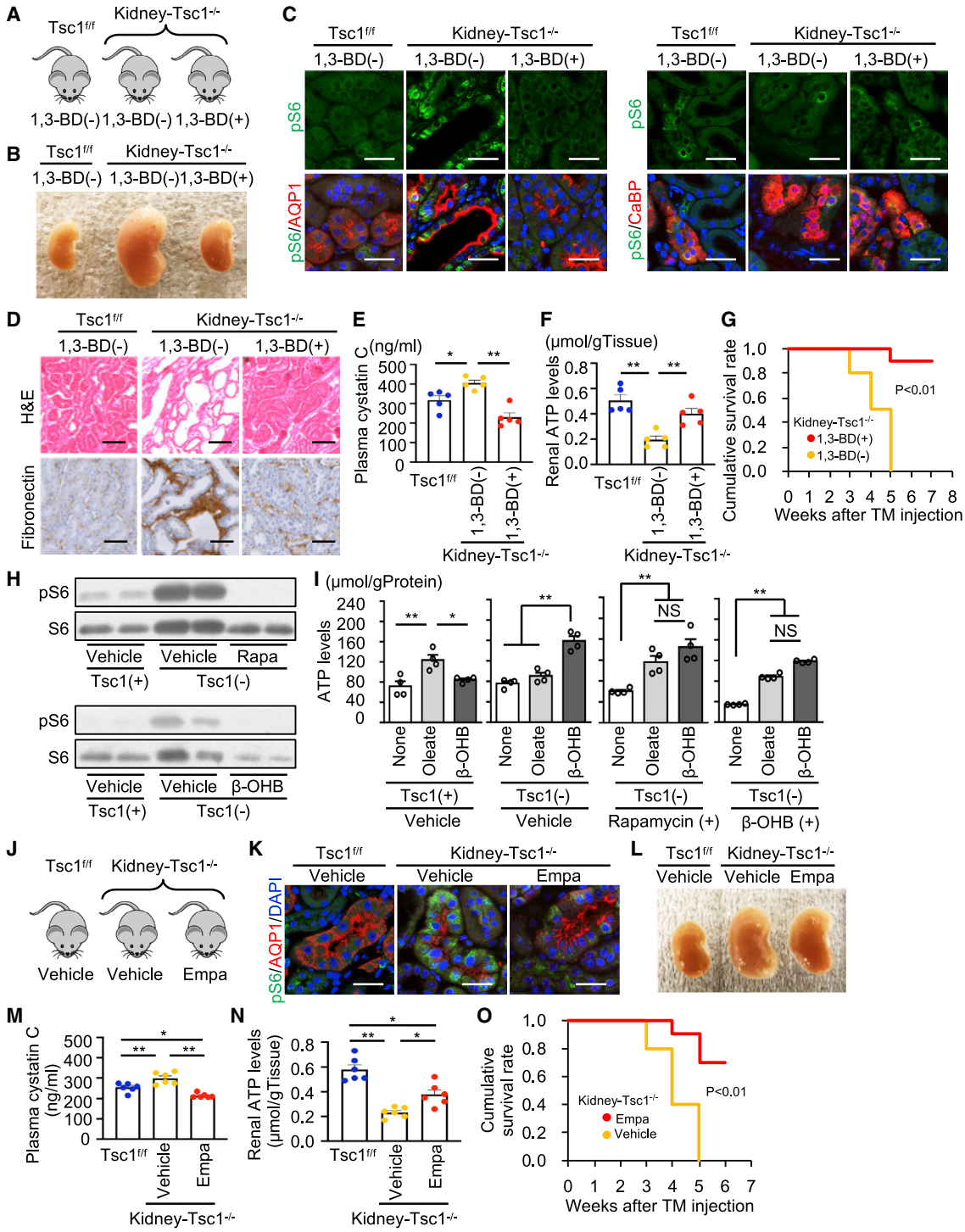

Figure 6. 1,3-BD and Empagliflozin Ameliorate Kidney Injury and the Mortality Rate in Tamoxifen-Inducible Kidney Tubule-Specific *Tsc-1* Knockout (Kidney-*Tsc1*$^{-/-}$) Mice

(A) Study protocol for examining the effect of 1,3-BD on the renal phenotype of kidney-specific *Tsc1*$^{-/-}$ mice.

(B) Macro renal morphology of the indicated groups.

(C) Immunofluorescence of pS6 in AQP1-positive PTECs and Calbindin D28k (CaBP)-positive distal tubules (scale bar, 50 μm).

(D) Representative images of H&E staining and immunostaining of fibronectin (scale bar, 50 μm) (n = 5 total samples per group analyzed).

(E and F) Plasma cystatin C (E) and ATP levels in renal cortex samples (F) (n = 5 per group).

(G) Cumulative survival rate in kidney-specific *Tsc1*$^{-/-}$ mice treated with or without 1,3-BD after tamoxifen-induced *Tsc1* deletion (n = 10 per group).

(H) Representative images of immunoblotting of pS6 and S6 in PTECs isolated from the indicated mouse groups (n = 8 total samples per group analyzed).

(legend continued on next page)

et al., 2012; Saxton and Sabatini, 2017). However, a direct interaction between ketone bodies and mTORC1 activity has not been demonstrated. In this study, β-OHB suppressed mTORC1 signaling directly in cultured *Tsc1*-deficient PTECs, and 1,3-BD dramatically improved the survival rate and reduced kidney injury in kidney-specific *Tsc1*$^{-/-}$ mice. Collectively, ketone bodies are likely to be endogenous inhibitors of mTORC1 signaling. Although the physiological significance of this interaction remains unclear, it may be globally involved in the benefits of caloric restriction.

Reprograming in renal energy metabolism, which is characterized by impaired lipolysis and enhanced ketolysis, was observed in the PTECs of HFD-fed *ApoE*$^{-/-}$ mice. Both impaired lipolysis and hyperactivation of mTORC1 were independently reported to be involved in the development of kidney diseases (Kang et al., 2015; Kuwagata et al., 2016). Our data connected the two major pathogenic changes. Hyperactivation of mTORC1 is responsible for impaired renal lipolysis in damaged PTECs, and in agreement with previous findings, mTORC1 hyperactivation plays a central role in impaired lipolysis in some metabolic tissues (Chakrabarti et al., 2013; Ricoult and Manning, 2013). Given that restoring lipolysis capacity has recently garnered greater attention as a therapeutic target for a variety of obesity-related metabolic diseases, the evidence that ketone bodies can improve lipolysis via mTORC1 inhibition should provide novel insights into this research area.

In addition to the effect of ketone bodies on kidney injury in the non-proteinuric DKD model, we examined its role in *db*/*db* mice, a proteinuric DKD model. The results showed that mTORC1-associated podocyte damage and massive proteinuria were attenuated by 1,3-BD and empagliflozin in *db*/*db* mice. Thus, ketone bodies may also be involved in the anti-proteinuric effect of SGLT2 inhibitors. Furthermore, ketone body supplementation prevented kidney injury by inhibiting mTORC1 signaling in non-diabetic 5/6 nephrectomized mice. Renoprotection by ketone bodies was accompanied by a blood pressure lowering effect, which is consistent with a previous report (Chakraborty et al., 2018). Enhanced ketogenesis, as well as enhanced natriuresis, may be involved in the anti-hypertensive effect of SGLT2 inhibitors. The results from the 5/6 nephrectomized mouse study further reinforce the concept that SGLT2 inhibitors are also effective drugs against non-diabetic kidney diseases.

Hyperactivation of mTORC1 is associated with a variety of diseases such as kidney, metabolic, and age-related diseases (Saxton and Sabatini, 2017). Recently, it was reported that ketone bodies stopped cyst formation in a rodent polycystic kidney disease model, which was accompanied by mTORC1 inhibition (Torres et al., 2019). Although evidence demonstrating an interaction between ketone bodies and mTORC1 signaling is still weak, and tissue-specific roles of ketone bodies in the regulation of mTORC1 signaling remain to be explored, it is possible that ketone body supplementation may become a promising therapeutic strategy against mTORC1-related diseases, including increasing longevity and improving metabolism in age-related diseases.

Local ketogenesis has recently been reported to be responsible for tissue repair in intestinal cells (Cheng et al., 2019). Given that PTECs can produce ketone bodies (Takagi et al., 2016) and SGLT2 inhibitors enhance renal ketogenesis (Kim et al., 2019), local ketogenesis in kidneys may be involved in renoprotection elicited by SGLT2 inhibitors. A kidney-specific *Hmgcs2*-deficient mouse model may verify this additional hypothesis. Revealing the roles of local ketone body production in kidney diseases may contribute to a better understanding of the pathogenesis of kidney diseases including DKD.

Pimozide is an antipsychotic drug currently in clinical use. Interestingly, a recent study demonstrated that this drug acted as a Scot inhibitor and reversed obesity-induced hyperglycemia in mice by blocking ketolysis in skeletal muscle (Al Batran et al., 2020). However, based on our results, blocking renal ketolysis may worsen kidney diseases. Thus, although no serious renal damage as a side effect of this drug has been clinically reported so far, whether this drug inhibits renal ketolysis and whether it adversely affects the long-term renal prognosis of subjects with chronic kidney disease may be an issue to be resolved in the future.

In conclusion, we provide a novel link between SGLT2 inhibition, renal ketone body metabolism, mTORC1 signaling, and DKD progression (Figure 7O). Although multiple mechanisms are expected to mediate the renoprotective effects elicited by SGLT2 inhibitors, its effects on ketone bodies and thus on damaged PTECs in the models examined here suggest that targeting renal energy metabolism may be a promising avenue in the treatment of both proteinuric and non-proteinuric DKD.

Limitations of Study

Although impaired renal lipolysis is mediated by mTORC1 activation, the mechanism underlying enhanced ketone body utilization in damaged kidneys remains unresolved (another aspect of renal energy reprograming in DKD). Based on our data, mTORC1 was not associated with this change. Some epigenetic factors, such as histone modifications, are reportedly associated with the pathogenesis of DKD (Kato and Natarajan, 2014), which may be involved in stimulated ketone utilization in damaged kidneys. Further examination to elucidate the mechanism underlying the upregulation of Scot expression in damaged kidneys is required. Second, the detailed molecular mechanism underlying ketone body-mediated inhibition of mTORC1 signaling remains unclear. Regulation of signals upstream of mTORC1, such as AMP-activated protein kinase and translocation of mTORC1 to lysosomal membranes, were previously reported to be regulatory mechanisms of mTORC1 activity (Inoki et al., 2012). These

(I) Energy dependency on oleate and β-OHB in isolated PTECs under the indicated conditions.
(J) Study protocol for examining the effect of empagliflozin on renal phenotypes of kidney-specific *Tsc1*$^{-/-}$ mice.
(K) Immunofluorescent study of pS6 in AQP1-positive PTECs (scale bar, 50 μm).
(L) Macro renal morphology in the indicated groups.
(M and N) Plasma cystatin C (M) and ATP levels in renal cortex samples (N) (n = 6 per group).
(O) Survival rate in kidney-specific *Tsc1*$^{-/-}$ mice treated with or without Empa after tamoxifen-induced *Tsc1* gene deletion (n = 10 per group).
Data are represented as mean ± SEM. *p < 0.05, **p < 0.01.

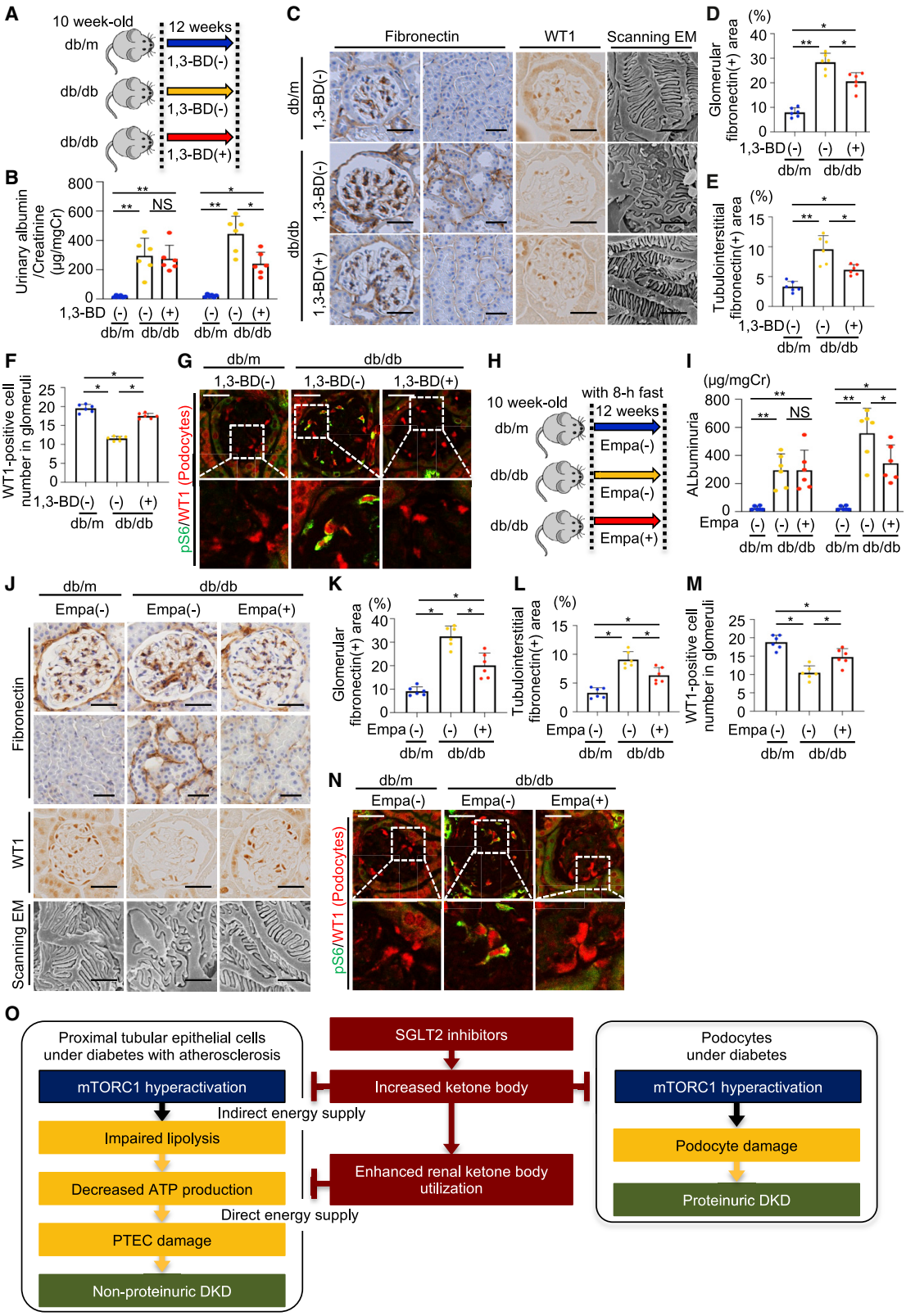

Figure 7. 1,3-BD Treatment and Empagliflozin Prevent Podocyte Injury and Massive Proteinuria in Type 2 Diabetic *db/db* Mice

(A) Study protocol for examining the effect of 1,3-BD on the renal phenotype of *db/db* mice.

(B) Albuminuria at start (left) and end (right) of the experiment (n = 6, each group).

(legend continued on next page)

mechanisms may be involved in ketone body-mediated mTORC1 inhibition. A more detailed mechanism of mTORC1-dependent impairment of renal lipolysis remains unclear, although an mTORC1-dependent decrease in lipolytic enzyme expression is likely to be involved. In addition, as mTORC1 regulates a variety of cellular functions, such as autophagy (Yamahara et al., 2013), changes in some cellular processes apart from lipolysis inhibition may be involved in mTORC1-mediated renal damage. As a technical concern, we cannot completely exclude the possibility that *Tsc1* deficiency or rapamycin affected pathways other than mTORC1, although these strategies have been widely used to activate and suppress mTORC1 signaling, respectively. Furthermore, clinical evidence showing an association between ketone body elevation in SGLT2 inhibitor treatment and DKD prognosis is still absent. Finally, the molecular mechanism by which SGLT2 inhibitors lead to upregulation of blood ketone body levels is still unclear. Solving these issues should provide further important insights into the pathogenesis of both metabolic and kidney diseases, and contribute to better renal prognosis of DKD.

STAR★METHODS

Detailed methods are provided in the online version of this paper and include the following:

- KEY RESOURCES TABLE
- RESOURCE AVAILABILITY
  - Lead Contact
  - Materials Availability
  - Data and Code Availability
- EXPERIMENTAL MODEL AND SUBJECT DETAILS
  - Mouse Models
  - Primary Cell Cultures
- METHOD DETAILS
  - En Face Analysis of Aorta
  - Renal Blood Flow Measurements
  - Histology
  - Measurement of Urinary Albumin
  - Measurement of Plasma Cystatin C
  - Measurement of ATP Levels in Renal Tissues
  - ATP Measurement in Cultured Cells
  - Immunoblots
  - Blood and Plasma Metabolic Parameters
  - Blood Pressure Measurement
- QUANTIFICATION AND STATISTICAL ANALYSIS
  - Statistical Analysis

SUPPLEMENTAL INFORMATION

Supplemental Information can be found online at https://doi.org/10.1016/j.cmet.2020.06.020.

ACKNOWLEDGMENTS

This study was supported by Grants-in-Aid for Scientific Research (KAKENHI) from the Japan Society for the Promotion of Science (18K08241 to S.K. and 17H06767 to N.O.), the SUMS President's Grant for the Encouragement of Young Researchers (to S.K.), a grant from Takeda Foundation (to S.K.), a Novartis Research Grant (to S.K.), an MSD Grant (to M.C.-K.), a JCR pharma (to S.-i.A.), the Japan Agency for Medical Research and Development (AMED) under grant numbers 19 gm1210009 and 19 gm5010002 (to M.Y.), and World Premier International Research Center Initiative (WPI), MEXT, Japan (to M.Y.). We thank Naoko Yamanaka and Keiko Kosaka (Shiga University of Medical Science) and the Central Research Laboratory of Shiga University of Medical Science for their technical assistance.

AUTHOR CONTRIBUTIONS

I.T., S.K., T.K., E.M., M.M., and H.M. designed the study. I.T., S.S., M.Y., and H.O. performed the experiments and established the gene-modified mouse models. I.T., S.K., S.S., N.O., K.Y., M.Y.-Y., N.T., M.C.-K., and S.-i.A. analyzed the data. I.T., S.K., T.K., E.M., M.M., S.-i.A., and H.M. drafted and revised the manuscript. All authors approved the final version of the manuscript.

DECLARATION OF INTERESTS

Part of this study was financially supported by Boehringer Ingelheim International GmbH (Ingelheim am Rheine, Germany) as a collaboration study. T.K. and E.M. were previous employees, and M.M. is a current employee of Boehringer Ingelheim Pharma.

Received: December 5, 2019
Revised: April 28, 2020
Accepted: June 26, 2020
Published: July 28, 2020

REFERENCES

Afkarian, M., Zelnick, L.R., Hall, Y.N., Heagerty, P.J., Tuttle, K., Weiss, N.S., and de Boer, I.H. (2016). Clinical manifestations of kidney disease among US adults with diabetes, 1988-2014. JAMA *316*, 602–610.

Al Batran, R., Gopal, K., Capozzi, M.E., Chahade, J.J., Saleme, B., Tabatabaei-Dakhili, S.A., Greenwell, A.A., Niu, J., Almutairi, M., Byrne, N.J., et al. (2020). Pimozide alleviates hyperglycemia in diet-induced obesity by inhibiting skeletal muscle ketone oxidation. Cell Metab. *31*, 909–919.e8.

Chakrabarti, P., Kim, J.Y., Singh, M., Shin, Y.K., Kim, J., Kumbrink, J., Wu, Y., Lee, M.J., Kirsch, K.H., Fried, S.K., and Kandror, K.V. (2013). Insulin inhibits lipolysis in adipocytes via the evolutionarily conserved mTORC1-Egr1-ATGL-mediated pathway. Mol. Cell. Biol. *33*, 3659–3666.

Chakraborty, S., Galla, S., Cheng, X., Yeo, J.Y., Mell, B., Singh, V., Yeoh, B., Saha, P., Mathew, A.V., Vijay-Kumar, M., and Joe, B. (2018). Salt-responsive

(C–F) Representative images of immunostaining of fibronectin and WT1 and scanning electron microscopic analysis of podocytes (scale bar, 50 μm for immunostaining, 2 μm for scanning EM) (C). Quantitative analysis of a fibronectin-positive area in glomeruli (D) and a tubulointerstitial lesion (E). WT1-positive podocyte number (F) (20 glomeruli per mouse were analyzed, n = 6, each group).
(G) Immunofluorescent study of pS6 in WT1-positive podocytes (scale bar, 50 μm).
(H) Study protocol for examining the effect of empagliflozin on the renal phenotype of *db/db* mice.
(I) Albuminuria at start (left) and end (right) of the experiment (n = 6, each group).
(J–M) Representative images of immunostaining of fibronectin and WT1 and scanning electron microscopic analysis of podocytes (scale bar, 50 μm for immunostaining, 2 μm for scanning EM) (J). Quantitative analysis of a fibronectin-positive area in glomeruli (K) and a tubulointerstial lesion (L). WT1-positive podocyte number (M) (20 glomeruli and 20 areas for tubulointerstial lesion per mouse were analyzed, n = 6, each group).
(N) Immunofluorescent study of pS6 in WT1-positive podocytes (scale bar, 50 μm).
(O) Schematic of our working hypothesis.
Data are represented as mean ± SEM. *p < 0.05, **p < 0.01. NS indicates no significance.

metabolite, β-hydroxybutyrate, attenuates hypertension. Cell Rep. *25*, 677–689.e4.

Cheng, C.W., Biton, M., Haber, A.L., Gunduz, N., Eng, G., Gaynor, L.T., Tripathi, S., Calibasi-Kocal, G., Rickelt, S., Butty, V.L., et al. (2019). Ketone body signaling mediates intestinal stem cell homeostasis and adaptation to diet. Cell *178*, 1115–1131.e15.

Cherney, D.Z.I., Zinman, B., Inzucchi, S.E., Koitka-Weber, A., Mattheus, M., von Eynatten, M., and Wanner, C. (2017). Effects of empagliflozin on the urinary albumin-to-creatinine ratio in patients with type 2 diabetes and established cardiovascular disease: an exploratory analysis from the EMPA-REG OUTCOME randomised, placebo-controlled trial. Lancet Diabetes Endocrinol. *5*, 610–621.

Cox, P.J., Kirk, T., Ashmore, T., Willerton, K., Evans, R., Smith, A., Murray, A.J., Stubbs, B., West, J., McLure, S.W., et al. (2016). Nutritional ketosis alters fuel preference and thereby endurance performance in athletes. Cell Metab. *24*, 256–268.

de Zeeuw, D., Remuzzi, G., Parving, H.H., Keane, W.F., Zhang, Z., Shahinfar, S., Snapinn, S., Cooper, M.E., Mitch, W.E., and Brenner, B.M. (2004). Proteinuria, a target for renoprotection in patients with type 2 diabetic nephropathy: lessons from RENAAL. Kidney Int. *65*, 2309–2320.

Dimitriadis, G.K., Nasiri-Ansari, N., Agrogiannis, G., Kostakis, I.D., Randeva, M.S., Nikiteas, N., Patel, V.H., Kaltsas, G., Papavassiliou, A.G., Randeva, H.S., and Kassi, E. (2019). Empagliflozin improves primary haemodynamic parameters and attenuates the development of atherosclerosis in high fat diet fed APOE knockout mice. Mol. Cell. Endocrinol. *494*, 110487.

Endo, T., Nakamura, J., Sato, Y., Asada, M., Yamada, R., Takase, M., Takaori, K., Oguchi, A., Iguchi, T., Higashi, A.Y., et al. (2015). Exploring the origin and limitations of kidney regeneration. J. Pathol. *236*, 251–263.

Ferrannini, E., Baldi, S., Frascerra, S., Astiarraga, B., Heise, T., Bizzotto, R., Mari, A., Pieber, T.R., and Muscelli, E. (2016). Shift to fatty substrate utilization in response to sodium-glucose cotransporter 2 inhibition in subjects without diabetes and patients with type 2 diabetes. Diabetes *65*, 1190–1195.

Gödel, M., Hartleben, B., Herbach, N., Liu, S., Zschiedrich, S., Lu, S., Debreczeni-Mór, A., Lindenmeyer, M.T., Rastaldi, M.P., Hartleben, G., et al. (2011). Role of mTOR in podocyte function and diabetic nephropathy in humans and mice. J. Clin. Invest. *121*, 2197–2209.

Han, J.H., Oh, T.J., Lee, G., Maeng, H.J., Lee, D.H., Kim, K.M., Choi, S.H., Jang, H.C., Lee, H.S., Park, K.S., et al. (2017). The beneficial effects of empagliflozin, an SGLT2 inhibitor, on atherosclerosis in ApoE $^{-/-}$ mice fed a western diet. Diabetologia *60*, 364–376.

Hess, D.A., Terenzi, D.C., Trac, J.Z., Quan, A., Mason, T., Al-Omran, M., Bhatt, D.L., Dhingra, N., Rotstein, O.D., Leiter, L.A., et al. (2019). SGLT2 inhibition with empagliflozin increases circulating provascular progenitor cells in people with type 2 diabetes mellitus. Cell Metab. *30*, 609–613.

Holman, R.R., Paul, S.K., Bethel, M.A., Matthews, D.R., and Neil, H.A. (2008). 10-year follow-up of intensive glucose control in type 2 diabetes. N. Engl. J. Med. *359*, 1577–1589.

Inoki, K., Mori, H., Wang, J., Suzuki, T., Hong, S., Yoshida, S., Blattner, S.M., Ikenoue, T., Rüegg, M.A., Hall, M.N., et al. (2011). mTORC1 activation in podocytes is a critical step in the development of diabetic nephropathy in mice. J. Clin. Invest. *121*, 2181–2196.

Inoki, K., Kim, J., and Guan, K.L. (2012). AMPK and mTOR in cellular energy homeostasis and drug targets. Annu. Rev. Pharmacol. Toxicol. *52*, 381–400.

Kamezaki, M., Kusaba, T., Komaki, K., Fushimura, Y., Watanabe, N., Ikeda, K., Kitani, T., Yamashita, N., Uehara, M., Kirita, Y., et al. (2018). Comprehensive renoprotective effects of ipragliflozin on early diabetic nephropathy in mice. Sci. Rep. *8*, 4029.

Kang, H.M., Ahn, S.H., Choi, P., Ko, Y.A., Han, S.H., Chinga, F., Park, A.S., Tao, J., Sharma, K., Pullman, J., et al. (2015). Defective fatty acid oxidation in renal tubular epithelial cells has a key role in kidney fibrosis development. Nat. Med. *21*, 37–46.

Kato, M., and Natarajan, R. (2014). Diabetic nephropathy–emerging epigenetic mechanisms. Nat. Rev. Nephrol. *10*, 517–530.

Kidokoro, K., Cherney, D.Z.I., Bozovic, A., Nagasu, H., Satoh, M., Kanda, E., Sasaki, T., and Kashihara, N. (2019). Evaluation of glomerular hemodynamic function by empagliflozin in diabetic mice using in vivo imaging. Circulation *140*, 303–315.

Kim, J.H., Lee, M., Kim, S.H., Kim, S.R., Lee, B.W., Kang, E.S., Cha, B.S., Cho, J.W., and Lee, Y.H. (2019). Sodium-glucose cotransporter 2 inhibitors regulate ketone body metabolism via inter-organ crosstalk. Diabetes Obes. Metab. *21*, 801–811.

Kume, S., Thomas, M.C., and Koya, D. (2012). Nutrient sensing, autophagy, and diabetic nephropathy. Diabetes *61*, 23–29.

Kume, S., Araki, S.I., Ugi, S., Morino, K., Koya, D., Nishio, Y., Haneda, M., Kashiwagi, A., and Maegawa, H. (2019). Secular changes in clinical manifestations of kidney disease among Japanese adults with type 2 diabetes from 1996 to 2014. J. Diabetes Investig. *10*, 1032–1040.

Kuwagata, S., Kume, S., Chin-Kanasaki, M., Araki, H., Araki, S., Nakazawa, J., Sugaya, T., Koya, D., Haneda, M., Maegawa, H., and Uzu, T. (2016). MicroRNA148b-3p inhibits mTORC1-dependent apoptosis in diabetes by repressing TNFR2 in proximal tubular cells. Kidney Int. *90*, 1211–1225.

Leelahavanichkul, A., Souza, A.C., Street, J.M., Hsu, V., Tsuji, T., Doi, K., Li, L., Hu, X., Zhou, H., Kumar, P., et al. (2014). Comparison of serum creatinine and serum cystatin C as biomarkers to detect sepsis-induced acute kidney injury and to predict mortality in CD-1 mice. Am. J. Physiol. Renal Physiol. *307*, F939–F948.

Lopaschuk, G.D., and Verma, S. (2016). Empagliflozin's fuel hypothesis: not so soon. Cell Metab. *24*, 200–202.

Ma, C., Zhang, W., Yang, X., Liu, Y., Liu, L., Feng, K., Zhang, X., Yang, S., Sun, L., Yu, M., et al. (2018). Functional interplay between liver X receptor and AMP-activated protein kinase α inhibits atherosclerosis in apolipoprotein E-deficient mice - a new anti-atherogenic strategy. Br. J. Pharmacol. *175*, 1486–1503.

Mazer, C.D., Hare, G.M.T., Connelly, P.W., Gilbert, R.E., Shehata, N., Quan, A., Teoh, H., Leiter, L.A., Zinman, B., Jüni, P., et al. (2020). Effect of empagliflozin on erythropoietin levels, iron stores, and red blood cell morphology in patients with type 2 diabetes mellitus and coronary artery disease. Circulation *141*, 704–707.

Mimura, I., and Nangaku, M. (2010). The suffocating kidney: tubulointerstitial hypoxia in end-stage renal disease. Nat. Rev. Nephrol. *6*, 667–678.

Mudaliar, S., Alloju, S., and Henry, R.R. (2016). Can a shift in fuel energetics explain the beneficial cardiorenal outcomes in the EMPA-REG OUTCOME study? A unifying hypothesis. Diabetes Care *39*, 1115–1122.

Neal, B., Perkovic, V., Mahaffey, K.W., de Zeeuw, D., Fulcher, G., Erondu, N., Shaw, W., Law, G., Desai, M., and Matthews, D.R.; CANVAS Program Collaborative Group (2017). Canagliflozin and cardiovascular and renal events in type 2 diabetes. N. Engl. J. Med. *377*, 644–657.

Neuen, B.L., Ohkuma, T., Neal, B., Matthews, D.R., de Zeeuw, D., Mahaffey, K.W., Fulcher, G., Li, Q., Jardine, M., Oh, R., et al. (2019). Effect of canagliflozin on renal and cardiovascular outcomes across different levels of albuminuria: data from the CANVAS Program. J. Am. Soc. Nephrol. *30*, 2229–2242.

Newman, J.C., Covarrubias, A.J., Zhao, M., Yu, X., Gut, P., Ng, C.P., Huang, Y., Haldar, S., and Verdin, E. (2017). Ketogenic diet reduces midlife mortality and improves memory in aging mice. Cell Metab. *26*, 547–557.e8.

Nielsen, R., Møller, N., Gormsen, L.C., Tolbod, L.P., Hansson, N.H., Sorensen, J., Harms, H.J., Frøkiær, J., Eiskjaer, H., Jespersen, N.R., et al. (2019). Cardiovascular effects of treatment with the ketone body 3-hydroxybutyrate in chronic heart failure patients. Circulation *139*, 2129–2141.

Puchalska, P., and Crawford, P.A. (2017). Multi-dimensional roles of ketone bodies in fuel metabolism, signaling, and therapeutics. Cell Metab. *25*, 262–284.

Ricoult, S.J., and Manning, B.D. (2013). The multifaceted role of mTORC1 in the control of lipid metabolism. EMBO Rep. *14*, 242–251.

Roberts, M.N., Wallace, M.A., Tomilov, A.A., Zhou, Z., Marcotte, G.R., Tran, D., Perez, G., Gutierrez-Casado, E., Koike, S., Knotts, T.A., et al. (2017). A ketogenic diet extends longevity and healthspan in adult mice. Cell Metab. *26*, 539–546.e5.

Sano, M., Takei, M., Shiraishi, Y., and Suzuki, Y. (2016). Increased hematocrit during sodium-glucose cotransporter 2 inhibitor therapy indicates recovery of tubulointerstitial function in diabetic kidneys. J. Clin. Med. Res. *8*, 844–847.

Saxton, R.A., and Sabatini, D.M. (2017). mTOR signaling in growth, metabolism, and disease. Cell *168*, 960–976.

Schugar, R.C., Moll, A.R., André d'Avignon, D., Weinheimer, C.J., Kovacs, A., and Crawford, P.A. (2014). Cardiomyocyte-specific deficiency of ketone body metabolism promotes accelerated pathological remodeling. Mol. Metab. *3*, 754–769.

Shimizu, M., Furuichi, K., Yokoyama, H., Toyama, T., Iwata, Y., Sakai, N., Kaneko, S., and Wada, T. (2014). Kidney lesions in diabetic patients with normoalbuminuric renal insufficiency. Clin. Exp. Nephrol. *18*, 305–312.

Singh, D.K., Winocour, P., and Farrington, K. (2008). Mechanisms of disease: the hypoxic tubular hypothesis of diabetic nephropathy. Nat. Clin. Pract. Nephrol. *4*, 216–226.

Takagi, A., Kume, S., Kondo, M., Nakazawa, J., Chin-Kanasaki, M., Araki, H., Araki, S., Koya, D., Haneda, M., Chano, T., et al. (2016). Mammalian autophagy is essential for hepatic and renal ketogenesis during starvation. Sci. Rep. *6*, 18944.

Tanaka, Y., Kume, S., Araki, S., Isshiki, K., Chin-Kanasaki, M., Sakaguchi, M., Sugimoto, T., Koya, D., Haneda, M., Kashiwagi, A., et al. (2011). Fenofibrate, a PPARα agonist, has renoprotective effects in mice by enhancing renal lipolysis. Kidney Int. *79*, 871–882.

Tanaka, S., Sugiura, Y., Saito, H., Sugahara, M., Higashijima, Y., Yamaguchi, J., Inagi, R., Suematsu, M., Nangaku, M., and Tanaka, T. (2018). Sodium-glucose cotransporter 2 inhibition normalizes glucose metabolism and suppresses oxidative stress in the kidneys of diabetic mice. Kidney Int. *94*, 912–925.

Torres, J.A., Kruger, S.L., Broderick, C., Amarlkhagva, T., Agrawal, S., Dodam, J.R., Mrug, M., Lyons, L.A., and Weimbs, T. (2019). Ketosis ameliorates renal cyst growth in polycystic kidney disease. Cell Metab. *30*, 1007–1023.e5.

Wang, Q., Zhang, M., Torres, G., Wu, S., Ouyang, C., Xie, Z., and Zou, M.H. (2017). Metformin suppresses diabetes-accelerated atherosclerosis via the inhibition of Drp1-mediated mitochondrial fission. Diabetes *66*, 193–205.

Wanner, C., Inzucchi, S.E., Lachin, J.M., Fitchett, D., von Eynatten, M., Mattheus, M., Johansen, O.E., Woerle, H.J., Broedl, U.C., and Zinman, B.; EMPA-REG OUTCOME Investigators (2016). Empagliflozin and progression of kidney disease in type 2 diabetes. N. Engl. J. Med. *375*, 323–334.

Winder, W.W., Baldwin, K.M., and Holloszy, J.O. (1974). Enzymes involved in ketone utilization in different types of muscle: adaptation to exercise. Eur. J. Biochem. *47*, 461–467.

Wiviott, S.D., Raz, I., Bonaca, M.P., Mosenzon, O., Kato, E.T., Cahn, A., Silverman, M.G., Zelniker, T.A., Kuder, J.F., Murphy, S.A., et al.; DECLARE–TIMI 58 Investigators (2019). Dapagliflozin and cardiovascular outcomes in type 2 diabetes. N. Engl. J. Med. *380*, 347–357.

Yamahara, K., Kume, S., Koya, D., Tanaka, Y., Morita, Y., Chin-Kanasaki, M., Araki, H., Isshiki, K., Araki, S., Haneda, M., et al. (2013). Obesity-mediated autophagy insufficiency exacerbates proteinuria-induced tubulointerstitial lesions. J. Am. Soc. Nephrol. *24*, 1769–1781.

Zhang, Y., Nakano, D., Guan, Y., Hitomi, H., Uemura, A., Masaki, T., Kobara, H., Sugaya, T., and Nishiyama, A. (2018). A sodium-glucose cotransporter 2 inhibitor attenuates renal capillary injury and fibrosis by a vascular endothelial growth factor-dependent pathway after renal injury in mice. Kidney Int. *94*, 524–535.

Zinman, B., Wanner, C., Lachin, J.M., Fitchett, D., Bluhmki, E., Hantel, S., Mattheus, M., Devins, T., Johansen, O.E., Woerle, H.J., et al.; EMPA-REG OUTCOME Investigators (2015). Empagliflozin, cardiovascular outcomes, and mortality in type 2 diabetes. N. Engl. J. Med. *373*, 2117–2128.

STAR★METHODS

KEY RESOURCES TABLE

REAGENT OR RESOURCE	SOURCE	IDENTIFIER
Antibodies		
Fibronectin	Millipore	Cat#AB2033; RRID: AB_2105702
F4/80	BIO-RAD	Cat#MCA497GA; RRID: AB_323806
Scot	Sigma Aldrich	Cat#HPA012047; RRID: AB_1854857
Hmgcs2	Cell Signaling Technology	Cat#20940; RRID: AB_2798853
CPT1A	Proteintech	Cat#15184-1-AP; RRID: AB_2084676
β actin	Sigma Aldrich	Cat#A5316; RRID: AB_476743
Phospho-S6 (Ser235/236)	Cell Signaling Technology	Cat#2211; RRID: AB_331679
S6 Ribosomal Protein (S6) (5G10)	Cell Signaling Technology	Cat#2217; RRID: AB_331355
ECL Anti-mouse IgG, Horseradish Peroxidase-Linked Whole Antibody	GE Healthcare	Cat#NA931; RRID: AB_772210
ECL Anti-Rabbit IgG, Horseradish Peroxidase-Linked Whole Antibody	GE Healthcare	Cat#NA934; RRID: AB_772206
CD31	Dianova GmbH	Cat#DIA-310; RRID: AB_2631039
Aquaporin 1	abcam	Cat#ab9566; RRID: AB_296494
Calbindin-D-28K	Sigma Aldrich	Cat#C9848; RRID: AB_476894
WT-1	Santa Cruz Biotechnology	Cat#sc-192; RRID: AB_632611
Chemicals, Peptides, and Recombinant Proteins		
Oil-Red O	Sigma Aldrich	Cat#MKCJ3586
Hematoxylin	Muto Kagaku	Cat#88529
Eosin	Muto Kagaku	Cat#32081
CLEA Rodent Diet CE-2 (Normal Diet)	CLEA Japan	CE-2
High fat diet 60%	ORIENTAL YEAST	N/A
Oleate	Sigma Aldrich	Cat#01008
Bovine serum albumin	Nakarai tesque	Cat#M7N0304
Collagenase Type II	Life Technologies	Cat#17104-019
Hyaluronidase	FUJIFILM Wako Pure Chemical Corporation	Cat# 37326-33-3
CELLection Biotin Binder Kit	Invitrogen	Cat#115332
Biotinylated Lotus Tetragonolobus Lectin (LTL)	VECTOR Laboratories	Cat#B-1325
β-hydroxybutylate	Sigma Aldrich	Cat#BCBM0192V
Rapamycin	LC Laboratories	Cat#53123-88-9
Empagliflozin	Boehringer Ingelheim GmbH	N/A
1,3-butanediol	Sigma Aldrich	Cat#SHBH3364V
Phosphatase inhibitor cocktail tablets	Sigma Aldrich	Cat#4906837001
Protease inhibitor cocktail tablets	Sigma Aldrich	Cat#11836145001
Tamoxifen	Sigma Aldrich	Cat#T4658-5G
Ethanol	Nakarai tesque	Cat#14713-53
Methanol	FUJIFILM Wako Pure Chemical Corporation	Cat#137-01823
0.5w/v% Methyl Cellulose 400 Solution, Sterilized	FUJIFILM Wako Pure Chemical Corporation	Cat#133-17815
Peroxidase Stain DAB kit	Nakarai tesque	Cat#25985-50
Cellstain-DAPI solution	Wako Pure Chemical Corporation	Cat#342-07431
Critical Commercial Assays		
LBIS Mouse Urinary Albumin Assay Kit (S-type)	FUJIFILM Wako Shibayagi Corporation	Cat# 638-25561
Urinary Creatinine ELISA Kit	FUJIFILM Wako Pure Chemical Corporation	Cat#301-35651
FFA assay kit	FUJIFILM Wako Pure Chemical Corporation	Cat#438-91691

(*Continued on next page*)

Continued

REAGENT OR RESOURCE	SOURCE	IDENTIFIER
TG assay kit	FUJIFILM Wako Pure Chemical Corporation	Cat# 467-08994
LDL-C assay kit	SEKISUI MEDICAL	Cat#261701
Cystatin C measurement kit	BioVendor	Cat#291009200R
TACS 2 TdT DAB kit	TREVIGEN	Cat#29274M13
AMERIC-ATP kit (For animal study)	AMERIC	Cat#AT002
IntraCellular ATP assay kit (For cell culture study)	TOYO INK GROUP	Cat#IC2-100
RELAR medium	CELL SCIENCE & TECHNOLOGY INSTITUTE	Cat#2112P05
Glutest Neo Alpha	Sanwa Kagaku	Cat#GT1830
PRECISION XCEED (ketometer)	Abbott	Cat#XEGS335-P03AF
hspCas9 mRNA	System Biosciences	Cat#CAS500A-1
T7 gRNA SmartNuclease Synthesis Kit	System Biosciences	Cat#CAS510A-KIT
mMESSAGE mMACHINER T7 Kit	Invitrogen	Cat#AM1344
Experimental Models: Organisms/Strains		
ApoE$^{+/-}$ mice	Jackson Laboratory	#002052
TSC1$^{f/f}$ mice	Jackson Laboratory	#005680
NDRG1-^{CreERT2} mice	Endo et al., 2015	N/A
Hmgcs2$^{-/-}$ mice	This paper	N/A
C57BL/6JJcl	CLEA Japan	N/A
BKS.Cg-m+/+Lepr^{db}*/Jcl (Db/m)*	CLEA Japan	N/A
BKS.Cg-+Lepr^{db}*/+Lepr*^{db}*/Jcl (Db/db)*	CLEA Japan	N/A
Other		
Polyvinylidene difluoride membranes	Merk Millipore	Cat#IPVH00010
2-dimentional laser blood flow imager, OMEGAZONE	OMEGAWAVE	Cat#OZ-3
Nikon Eclipse 90i (microscope)	Nikon Corporation	N/A
NanoDrop 1000 Spectrophotometer	Thermo Fisher Scientific	N/A
Image-Pro Plus (version 7.0)	Media Cybernetics	N/A
SPSS software (version 22)	IBM	N/A
White Light Laser Confocal Microscope Leica TCS SP8 X	Leica MICROSYSTEMS	N/A
COMPACT pH METER (LAQUAtwin-pH-22B)	HORIBA Advanced Techno	N/A
BP-98A-L (Blood pressure monitor)	Softron	N/A
Transmission Electron Microscope H-7500	Hitachi High-Tech Corporation	N/A
Scanning Electron Microscope JSM-7800F	JEOL	N/A
Prism 8 (version 4.1)	GraphPad	N/A

RESOURCE AVAILABILITY

Lead Contact

Further information and requests for resources and reagents should be directed to and will be fulfilled by the Lead Contact, Shinji Kume (skume@belle.shiga-med.ac.jp).

Materials Availability

Mouse lines generated in this study (*Hmgcs2*$^{-/-}$ mice) are available from the lead contact upon request.

Data and Code Availability

There are neither new datasets/code generated nor restrictions for use of the materials in the paper.

EXPERIMENTAL MODEL AND SUBJECT DETAILS

Mouse Models

All experimental protocols were approved by the Gene Recombination Experiment Safety Committee and Research Center for Animal Life Science (RCALS) at Shiga University of Medical Science. All mice were housed in a temperature-controlled environment

(23°C) with a 12-h light and 12-h dark (20:00–08:00) photoperiod, and cared for in facilities operated by Research Center for Animal Life Science at Shiga University of Medical Science. CLEA Rodent Diet (#CE-2, CLEA Japan) was used as the standard chow in the center. Mice housed in the center are regularly tested for health conditions, including microbacterial inspection.

Eight-week old male and female *ApoE*$^{+/-}$ mice were purchased from Jackson Laboratory (#002052, B6.129P2-*Apoe*^{tm1Unc}/J; Bar Harbor, ME, USA). *ApoE*$^{-/-}$ mice (C57BL/6 background) were generated by crossbreeding male and female *ApoE*$^{+/-}$ mice. Ten-week-old male *ApoE*$^{-/-}$ mice and their littermate controls *ApoE*$^{+/+}$ mice were fed a 60% high-fat diet (HFD) or normal diet (ND), respectively, for 24 weeks, and atherosclerosis, renal blood flow, renal histology, and renal function were examined after sacrifice.

For the study of 1,3-butanediol (1,3-BD) treatment in HFD-fed *ApoE*$^{-/-}$ mice, 1,3-BD was administered by preparing a HFD containing 20% 1,3-BD solution (Sigma Aldrich, St. Louis, MO, USA). First, 10-week old male *ApoE*$^{-/-}$ mice were fed a 60% HFD for 16 weeks (n = 13), and then fed either a 1,3-BD-containing HFD (n = 6) or a simple HFD (n = 7). Age-matched ND-fed *ApoE*$^{+/+}$ mice were used as a control group (n = 5).

For the study of empagliflozin treatment in HFD-fed *ApoE*$^{-/-}$ mice, 10-week old male *ApoE*$^{-/-}$ mice were fed a 60% HFD for 16 weeks (n = 16) and then orally administrated with empagliflozin (30 mg/kg/day, n = 8) or vehicle solution (n = 8) for 8 weeks. In this study, oral gavage was performed at 17:00, and all mice were fasted from 09:00 to 17:00 to match the rhythm of their daily lives to general human subjects. Age-matched ND-fed *ApoE*$^{+/+}$ mice were used as a control group (n = 5). Empagliflozin compound was first resolved in methanol (30 mg/mL) and then diluted in 0.5% (w/v) methylcellulose solution at a final concentration of 3 mg/mL. Methanol in 0.5% (w/v) methylcellulose was used as the vehicle.

A mouse model harboring a deletion mutation in exon 2 of the mouse *Hmgcs2* gene was generated using the Crispr/Cas9 system at Unitech (Chiba, Japan). Cas9 mRNA and single guide RNAs (sgRNAs) were synthesized as follows. Cas9 mRNA was prepared *in vitro* from linear DNA templates using the CAS500A-1 hspCas9 mRNA (System Biosciences, Palo Alto, CA), and sgRNAs were generated using the CAS510A-KIT T7 gRNA SmartNuclease Synthesis Kit (System Biosciences) and AM1344 mMESSAGE mMACHINER T7 Kit (Invitrogen, Carlsbad, CA, USA), according to the manufacturer's instructions. The following sequences were used for sgRNA synthesis: sgRNA1, TGGAACGCACAAAGCTGCCG; sgRNA2, GTGCCTGCAGTGGTACAGA. Cas9 mRNA and sgRNAs (CAS9 mRNA: gRNA1gg:gRNA2cc = 2:1:1) were microinjected into fertilized embryos of C57BL/6J mice. Mouse lines with mutations in the mouse *Hmgcs2* gene were confirmed. Among these, one mouse line with a 38-bp deletion mutation in exon 2, which led to a frameshift and subsequent complete deletion of Hmgcs2 protein synthesis, was selected for use in our study. Mutations in *Hmgcs2* were confirmed by Sanger sequencing analyses (Bionics, Gangwon-do, South Korea). Homozygous *Hmgcs2*$^{-/-}$ mice were born from a heterozygous intercross and used for phenotypic analyses in parallel with age- and sex-matched wild-type littermates as a control group. All mice were genotyped 2 weeks after birth by PCR with specific primers (forward, 5′-AATATGTGGACCAAACTGACCTG-3′ and reverse, 5′-CTTGGACTTGTCAATGATGGTCT-3′). Animals were housed according to their sex after weaning. Functional deletion of the gene was confirmed by a deficient ketone body increase during 36-h fasting in *Hmgcs2*$^{-/-}$ mice. Double-knockout mice lacking murine *ApoE* and *Hmgcs2* genes were generated by crossbreeding male and female *ApoE*$^{-/-}$-*Hmgcs2*$^{+/-}$ mice.

For the study of empagliflozin treatment in *ApoE*$^{-/-}$ mice and *ApoE*$^{-/-}$ mice lacking the *Hmgcs2* gene, 10-week old male *ApoE*$^{-/-}$ mice (n = 15) and *ApoE*$^{-/-}$ mice lacking the *Hmgcs2* gene (n = 7) were fed with a 60% HFD for 16 weeks. Subsequently, *ApoE*$^{-/-}$ mice fed a HFD for 16 weeks were treated with either empagliflozin (30 mg/kg/day, n = 7) or vehicle solution (n = 8). *ApoE*$^{-/-}$ mice lacking the *Hmgcs2* gene were all treated with empagliflozin (30 mg/kg/day). The protocol for empagliflozin administration was as described above.

Tsc1$^{f/f}$ mice (C57BL/6 background) were purchased from Jackson Laboratory (#005680, STOCK *Tsc1*^{tm1Djk}/J). The *Ndrg1*^{CreER} mouse model (C57BL/6 background) was previously established by Motoko Yanagita's lab (Endo et al., 2015). *Tsc1*$^{f/f}$-*Ndrg1*^{CreER} mice were generated by crossbreeding female *Tsc1*$^{f/f}$ mice and male *Ndrg1*^{CreER} mice. Subsequently, female *Tsc1*$^{f/f}$ mice and male *Tsc1*$^{f/+}$ mice carrying *Ndrg1*^{CreER} were crossbred to obtain *Tsc1*$^{f/f}$ mice carrying *Ndrg1*^{CreER}. Eight-week-old *Tsc1*$^{f/f}$ mice and *Tsc1*$^{f/f}$ mice carrying *Ndrg1*^{CreER} were intraperitoneally injected with 150 mg/kg/day of tamoxifen for 5 consecutive days. Male tamoxifen-injected *Tsc1*$^{f/f}$ mice were used as controls. To evaluate survival rates, male kidney-specific *Tsc1*$^{-/-}$ mice (Kidney-*Tsc1*$^{-/-}$ mice; tamoxifen-injected *Tsc1*$^{f/f}$ mice carrying *Ndrg1*^{CreER}) were divided into two groups: 1,3-BD treatment (n = 10) and non-treatment (n = 10). 1,3-BD treatment was started at the time of tamoxifen-induced Cre induction. Survival rates were assessed until 8 weeks after tamoxifen injection. In another series of studies, living PTEC-*Tsc1*$^{-/-}$ mice treated with or without 1,3-BD were examined for renal phenotypes in three groups (n = 5 per group), and were analyzed at 4 weeks after tamoxifen-induced Cre induction. To examine the effect of empagliflozin, male Kidney-*Tsc1*$^{-/-}$ mice were treated with or without empagliflozin (n = 6 for analyzing renal phenotype at 4 weeks after tamoxifen injection, and n = 10 for evaluating survival rate). The protocol for empagliflozin gavage was as described above.

Eight-week old *db*/*db* mice (BKS background) were purchased from Clea Japan (Tokyo, Japan) and used for 1,3-BD treatment experiments. 1,3-BD was administered by preparing ND containing a 20% 1,3-BD solution. Eight-week old male diabetic *db*/*db* mice were fed ND for two weeks and then fed either a 1,3-BD-containing diet (n = 6) or simple ND (n = 6) for a further 12 weeks. Age-matched ND-fed *db*/*m* mice were used as a control group (n = 6).

To study empagliflozin treatment of *db*/*db* mice, eight-week-old male *db*/*db* mice were fed ND for two weeks and then orally administrated with empagliflozin (30 mg/kg/day, n = 6) or vehicle solution (n = 6) for 12 weeks. In this study, oral gavage was performed at 17:00, and all mice were fasted from 09:00 to 17:00 to match the rhythm of their daily lives to general human subjects. Age-matched *db*/*m* mice fed ND were used as a control group (n = 6).

Seven-week-old male C57BL/6 mice were purchased from Clea Japan (Tokyo, Japan) for the study of 5/6 nephectomized mice. After a week, ligation-based 2/3 nephrectomy in the left kidney was performed on eight-week-old male C57BL/6 mice as a first operation. The superior and inferior 1/3 parts of the kidney were ligated with a 3-0 silk suture string. Seven days later, the right kidney was removed. For the sham surgery, the same surgical procedures were performed, including exposure of the kidney, dissection of tissue, and wound closure, but without the pole ligation of the left kidney or removal of the right kidney. Nine-week-old operated mice were treated with 1,3-BD or empagliflozin using the same protocol as described above for the *db*/*db* mouse study. Seven mice were prepared for each mouse group.

For sacrificing, mice were anesthetized, and blood samples were drawn by ventricular puncture. Next, mice were perfused with phosphate-buffered saline (PBS) and the unilateral kidney was removed. Finally, mice were perfused with fixative buffer (4% paraformaldehyde in 0.1 M phosphate buffer), and the fixed kidneys and aorta were removed. Blood samples were collected into heparin-coated tubes and centrifuged to collect plasma samples, which were stored at −80°C until assays. Renal cortexes were isolated from kidneys (removed after PBS infusion) and frozen in liquid nitrogen, while frozen cortexes were used for immunoblots and ATP measurements. Fixed kidney tissues were used for hematoxylin and eosin (H&E) staining, immunostaining, and terminal deoxynucleotidyl transferase dUTP nick end labeling (TUNEL) staining. For en face aorta analyses, aorta samples were pinned on a black wax surface, fixed, and stained with Oil-Red O. Details for each assay are described in the Method Details section.

Primary Cell Cultures

All cells were grown at 37°C in a 5% CO2 humid atmosphere. Male HFD-fed *ApoE*$^{-/-}$ mice and male ND-fed *ApoE*$^{+/+}$ mice aged 34 weeks, as well as 12-week old male *Tsc1*$^{f/f}$ mice carrying Cre recombinase in PTECs, were used for the PTEC isolation study. After anesthetization, the kidneys were immediately removed and placed in cold (4°C) phosphate buffer. The renal capsule was removed and the kidney was sagittally cut into two halves. The medulla was dissected and discarded from each half. The remaining cortical tissue was minced and digested in Hanks' balanced salt solution containing collagenase type II (Life Technologies, Carlsbad, CA, USA; 200 units/mL) and hyaluronidase (Wako Pure Chemical Industries, Osaka, Japan; 0.2%). Tubules were incubated at 37°C while rotating for 2 h. After digestion, the tubule suspension was centrifuged at 200 × g for 5 min. The selection of PTECs was performed using a CELLection Biotin Binder Kit (Invitrogen) and biotinylated *Lotus tetragonolobus* agglutinin lectin (LTL) (Vector Laboratories, Burlingame, CA, USA). Isolated PTECs were resuspended in RELAR medium (Cell Science & Technology Institute, Sendai, Japan) and seeded into culture dishes.

METHOD DETAILS

En Face Analysis of Aorta

Isolated aorta samples placed on a black wax surface for en face analysis were fixed in 4% paraformaldehyde, 5% sucrose, and 20 μmol EDTA (pH 7.4). Lipids were visualized with standard Oil-Red O staining (Thermo Fisher Scientific, Waltham, MA, USA). Images were acquired, and the percentage of aortic area stained red was determined using image analysis software (Image Pro, Media Cybernetics, Rockville, MD, USA). Data are expressed as the percentage of red-colored area to the total observed aortic area.

Renal Blood Flow Measurements

Renal blood flow in living mice were measured using a laser speckle blood flow imager (Omega Zone; Omegawave, Espoo, Finland) under anesthesia with 1.5% isoflurane. For each mouse, renal blood flow was measured in three different areas within one kidney, and the average value was taken as the renal blood flow of that individual.

Histology

The removed renal tissues were fixed with 4% paraformaldehyde for 24 h, dehydrated with a decreasing alcohol series (2 × 100%, 2 × 95%, 2 × 70%, 2 × toluene) for 2 h each, and finally immersed in paraffin for 6 h twice. Paraffin-embedded renal samples were sectioned (3 μm) and subjected to standard H&E and PAS staining. The stained sections were observed with a Nikon Eclipse 90i microscope (Nikon Corporation). From each mouse, 20 glomeruli cut at their vascular poles were supplied for morphometrical analysis. The glomerular tuft area (glomerular size) and the extent of the mesangial matrix (mesangial area) were determined by assessing the PAS-positive, and the nuclei-free area in the mesangium was analyzed using a computer-assisted color image analyzer (Image-pro plus v. 7, Nippon Roper, Tokyo, Japan).

For immunostaining, paraffin-embedded tissue sections were used. Endogenous peroxidases were blocked with 0.03% H_2O_2 for 10 min and nonspecific binding was blocked with 2% normal goat serum for 30 min. Tissues were incubated with primary antibody for 12 h at 4°C, followed by incubation with ImmPRESS HRP Anti-Rabbit IgG Polymer Detection Kit (Vector Laboratories) according to the manufacturer's recommendations. Reactions were developed with Peroxidase Stain DAB kit (Nakarai Tesque, Kyoto, Japan) according to the manufacturer's instructions, and then slides were counterstained with hematoxylin. To analyze the stain-positive area of fibronectin in glomerular and tubulointerstitial lesions and CD31-positive vascular density in the interstitium, a tissue photograph at a magnification of 200 was used, and the ratio of the area showing density higher than the lower limit of positivity was calculated using Image-Pro Plus (version 7.0) (Media Cybernetics). For analyzing F4/80 positive cell number, nuclei number of F4/80-positive cells in the interstitium were counted in a tissue photograph at a magnification of 200. For quantitative analysis, 20 areas were analyzed per mouse kidney sample.

TUNEL staining was performed using a TACS 2 TdT DAB Kit (Trevigen, Gaithersburg, MD, USA) according to the manufacturer's instructions. At least 20 cortical areas at a magnification of 200 were imaged and numbers of TUNEL-positive cells in tubular cells were counted. Data are expressed as numbers of TUNEL-positive cells per visual field.

For the immunofluorescent study, fixed kidney sections were preincubated with 2% BSA in PBS for 10 min at room temperature. The samples were then covered overnight at 4°C with the primary antibody in the pre-incubation solution. The sections were rinsed three times with PBS, incubated with 2% goat serum in 2% BSA in PBS at room temperature, and then incubated for 1 h at 4°C with the secondary antibodies. After DAPI staining and subsequent rinsing with PBS, the sections were mounted using mounting medium. The stained sections were imaged with a fluorescence microscope (White Light Laser Confocal Microscope Leica TCS SP8 X, Leica MICROSYSTEMS, Wetzlar, Germany).

For electron microscopic analysis, after fixation with 2% osmium tetroxide, kidney tissues were dehydrated in a series of graded ethanol preparations, ethanol was replaced with propylene oxide, and samples were embedded in epoxy resin. Ultrathin sections were double-stained with uranyl acetate and lead. Transmission and scanning electron microscopic analyses were performed using a Hitachi S-570 and H-7500 instrument (Hitachi, Tokyo, Japan).

Measurement of Urinary Albumin

Urine samples were collected over the course of 24 h using metabolic cages in which mice were able to freely access food and water. Collected urine samples were centrifuged to remove debris. Clear supernatants of urine samples were used to measure albumin and creatinine concentrations using an LBIS Mouse Urinary Albumin Assay Kit (S-type) (FUJIFILM Wako Shibayagi Corporation, Tokyo, Japan) and Urinary Creatinine ELISA Kit (FUJIFILM Wako Pure Chemical Corporation), respectively, according to the manufacturers' instructions. Urinary albumin levels are reported as the ratio of urinary albumin to creatinine.

Measurement of Plasma Cystatin C

Plasma cystatin C levels were measured using a Cystatin C measurement kit (BioVender, Asheville, NC, USA) according to the manufacturer's instructions.

Measurement of ATP Levels in Renal Tissues

ATP concentrations in renal cortex samples were measured using an AMERIC-ATP Kit (AMERIC, Tokushima, Japan), according to the manufacturer's instructions. AUTO-LUMINOCOUNTER (Microtec, Funabashi, Japan) was used to measure luminescence. ATP concentrations are expressed as the ratio of ATP concentration to tissue volume.

ATP Measurement in Cultured Cells

Seven days after seeding isolated cells, the cell culture medium was changed to Krebs-Ringer buffer without glucose and then either 200 mM oleate or 10 mM β-hydroxybutyrate (β-OHB) was added for 3 h. Untreated cells and cells treated with either oleate or β-OHB were harvested with the extraction solution provided in the Intracellular ATP Assay Kit (Toyo Ink Group, Tokyo, Japan). ATP concentration was measured using the kit according to the manufacturer's instructions and expressed as the ratio of ATP concentration to protein concentration in samples.

For cell culture study to examine the effect of *Tsc1* deficiency on energy dependency, isolated PTECs from *Tsc1*$^{f/f}$ mice carrying Cre recombinase were treated with/without tamoxifen (250 nM) to induce Cre expression from day 3 to day 7 after the isolation. For rapamaycin treatment in the isolated PTECs from HFD-fed ApoE$^{-/-}$ or TSC1$^{f/f}$ mice carrying Cre recopmbinase, the cells were treated with rapamycin (1 pg/mL) for 24 h prior to assays of immunoblot or ATP measurement assay.

Immunoblots

Samples from the cultured cells seeded for 7 days after the isolation, and renal cortex samples were homogenized in ice-cold lysis buffer containing 4% sodium dodecyl sulfate (SDS), 100 mM Tris (pH 6.8), phosphatase inhibitor cocktail 2 and 3, and protease inhibitor cocktail (Sigma Aldrich). Samples were vortexed and heated at 100°C for 5 min, followed by vortexing and centrifugation to remove undissolved debris. Protein concentrations were estimated by measuring the absorbance at 280 nm using a NanoDrop spectrometer (Thermo Fisher Scientific). Samples were resolved by SDS-polyacrylamide gel electrophoresis and transferred to polyvinylidene fluoride membranes (Immobilon; EMD Millipore, Burlington, MA, USA). After the membranes were blocked in 5% skim milk or 5% bovine serum albumin for 30 min at room temperature, they were incubated with primary antibodies overnight at 4°C, followed by incubation with the corresponding secondary antibodies for 1 h at room temperature. Information on antibodies is listed in the Key Resources Table. All primary antibodies were used at a dilution of 1:1000, with the exception of β-actin and pS6 (1:10000). Membranes were washed and incubated with horseradish peroxidase-coupled secondary antibodies (1:1000; Amersham Biosciences, Little Chalfont, UK). Blots were visualized with an enhanced chemiluminescence detection system (Perkin Elmer, Waltham, MA, USA). Full gel scan images are shown in Figure S7.

Blood and Plasma Metabolic Parameters

Glucose and ketone body concentrations in blood collected from the tail vein were measured using a Glutest sensor (Sanwa Kagaku Kenkyusho, Nagoya, Japan) and Ketometer (Abbott, Chicago, IL, USA), respectively. The plasma pH was measured using a Compact

pH meter (Horiba Advanced Techno, Kyoto, Japan). Free fatty acids, triglycerides, and low-density lipoprotein cholesterol were measured using specific assay kits according to the manufacturer's instructions.

Blood Pressure Measurement

Conscious mice were placed on a heated pad (37°C) in a temperature-controlled quiet room to measure their blood pressure. After 5 min of resting conditions, the systolic blood pressure was measured using a programmable tail-cuff sphygmomanometer (BP98-A; Softron, Tokyo, Japan). Ten consecutive measurements of each mouse were collected, and the average values were calculated.

QUANTIFICATION AND STATISTICAL ANALYSIS

Statistical Analysis

For comparison among multiple groups, two-way ANOVA followed by Tukey's post hoc analysis was used to determine the effect of genotype and treatment. For comparison between two groups, an unpaired Student's t test was used. Associations between plasma cystatin C levels and renal ATP contents were analyzed using Pearson's correlation coefficient. Survival parameters in the study using *Tsc1*$^{-/-}$ mice were determined using the Kaplan-Meier method and compared using log-rank tests. In all analyses, Prism 8 version 4.1 (GraphPad) was used, and p values < 0.05 were considered statistically significant. Experimenters were not blinded to the treatment or genotypes of animals; however, semiquantitative analysis of renal histology was conducted blinded. Exclusion criteria were based on animal well-being at the beginning of the study. No animals were excluded from this study. No power analysis was performed to determine the sample size. The sample size in each study was based on experience with previous studies employing DKD animals and knockout mice in our lab.